Published in final edited form as:

Nature. 2020 November ; 587(7832): 121–125. doi:10.1038/s41586-020-2850-3.

Cancer Immunotherapy via Targeted TGF-β Signaling Blockade in T_H Cells

Shun Li[1], **Ming Liu**[1], **Mytrang H. Do**[1,2], **Chun Chou**[1], **Efstathios G. Stamatiades**[1], **Briana G. Nixon**[1,2], **Wei Shi**[1], **Xian Zhang**[1], **Peng Li**[1], **Shengyu Gao**[1,3], **Kristelle J. Capistrano**[1], **Hong Xu**[4], **Nai-Kong V. Cheung**[4], **Ming O. Li**[1,2,3,*]

[1]Immunology Program, Sloan Kettering Institute, Memorial Sloan Kettering Cancer Center, New York, NY, USA 10065

[2]Immunology and Microbial Pathogenesis Program, Weill Cornell Graduate School of Medical Sciences, Cornell University, New York, NY, USA 10065

[3]Louis V. Gerstner Jr Graduate School of Biomedical Sciences, Memorial Sloan Kettering Cancer Center, New York, NY, USA 10065

[4]Department of Pediatrics, Memorial Sloan Kettering Cancer Center, New York, NY, USA 10065

Abstract

Cancer arises from malignant cancer cells in dynamic multilevel interactions with the host tissue. Cancer therapies aiming to directly destruct cancer cells including oncogene-targeted therapy and immune checkpoint therapy that revives tumor-reactive cytotoxic T lymphocytes are effective in some patients[1,2]; yet, acquired resistance frequently ensues[3,4]. An alternative therapeutic strategy aspires to rectify the host tissue pathology including vasculature abnormalities that foster cancer progression[5,6]; however, neutralization of proangiogenic factors such as vascular endothelial growth factor A (VEGFA) has limited clinical benefits[7,8]. Following the finding that transforming growth factor-β (TGF-β) suppresses T helper 2 (Th2)-mediated cancer immunity (cite accompanying paper from Liu M *et al.*), here we show that blocking TGF-β signaling in $CD4^+$ T cells remodels the tumor microenvironment and restrains cancer progression. In a murine model of breast cancer resistant to immune checkpoint or anti-VEGF therapies[9,10], inducible genetic deletion of the TGF-β receptor II (TGF-βRII) in $CD4^+$ T cells suppressed tumor growth. For pharmacological blockade, we engineered a bispecific receptor decoy by attaching the TGF-β-neutralizing TGF-βRII extracellular domain to ibalizumab, a non-immunosuppressive CD4 antibody[11,12], naming it CD4 TGF-β Trap (4T-Trap). Compared to a non-targeted TGF-β-Trap, 4T-Trap selectively inhibited Th cell TGF-β signaling in tumor-draining lymph nodes, causing

*Correspondence: lim@mskcc.org.

Author Contributions

S.L. and M.O.L. were involved in all aspects of this study, including planning and performing experiments, analysis and interpretation of data and writing the manuscript. M.L. and M.O.L. initiated the project. M.L. performed experiments on proliferation of cancer cells, angiogenesis in tumor tissues and inducible TGF-βRII deletion in PyMT mice, interpreted data and wrote the manuscript. H.X. assisted S.L. for the Biacore assays and interpretation of data. K.J.C., S.G., P.L., B.G.N., W.S., X.Z., C.C., M.H.D. and E.G.S. assisted with mouse colony management and performed experiments.

Competing Interests

MSKCC has filed a patent application with the U.S. Patent and Trademark Office directed toward methods and compositions for targeting TGF-β signaling in $CD4^+$ helper T cell for cancer immunotherapy.

tumor vasculature reorganization and cancer cell death, a process dependent on the Th2 cytokine interleukin-4 (IL-4). Notably, the 4T-Trap-induced tumor tissue hypoxia led to increased VEGFA expression. VEGF inhibition enhanced the starvation-triggered cancer cell death and amplified the anti-tumor effect of 4T-Trap. Thus, targeted TGF-β signaling blockade in helper T cells elicits an effective tissue-level cancer defense response that can anchor the cancer environment-directed therapies.

Cancer evolves from aberrant cancer cell and stroma interactions rooted in the maladaptation of developmental and tissue maintenance programs such as embryogenesis and wound healing[13,14]. Notably, tumor neovasculature resembles that of chronic wounds and fosters cancer progression[15]. We are interested in exploring immunological means of tumor vasculature reprogramming and have focused on the MMTV-PyMT (PyMT) transgenic model of murine breast cancer. Immunohistological analyses revealed that sprouting angiogenesis increased substantially early on when mammary tumors reached a size of 5x5 mm in association with cancer cell proliferation (Fig. 1a and Extended Data Fig. 1a). Torturous and bluntly ended vasculature became more abundant in later stage 9x9 mm tumors, accompanied by further enhanced cancer cell proliferation (Fig. 1a and Extended Data Fig. 1a).

Constitutive inhibition of TGF-β signaling in $CD4^+$ T cells remodels the tumor vasculature and suppresses cancer progression (cite accompanying paper from Liu M *et al.*). To probe its therapeutic potential, we crossed PyMT mice carrying a floxed allele of the *Tgfbr2* gene (*Tgfbr2*$^{fl/fl}$) with $CD4^{CreERT2}$ transgenic mice in which the Cre recombinase could be activated in $CD4^+$ T cells by tamoxifen[16]. Cohorts of $CD4^{CreERT2}$ *Tgfbr2*$^{fl/fl}$PyMT and control *Tgfbr2*$^{fl/fl}$PyMT mice bearing 5x5 mm tumors were left untreated or treated with tamoxifen and monitored for tumor growth. Tamoxifen treatment of $CD4^{CreERT2}$ *Tgfbr2*$^{fl/fl}$PyMT mice ablated TGF-βRII expression specifically in $CD4^+$ T cells (Extended Data Fig. 1b), causing enhanced differentiation of interferon-γ (IFN-γ)-producing Th1 and IL-4-producing Th2 cells (Extended Data Fig. 1c). Tumor burden was reduced by 5-fold at 6 weeks post-treatment in $CD4^{CreERT2}$ *Tgfbr2*$^{fl/fl}$PyMT mice (Fig. 1b), associated with increased cancer cell death, while cancer cell proliferation was unaffected (Extended Data Fig. 1d). Compared to tumors from tamoxifen-treated *Tgfbr2*$^{fl/fl}$PyMT mice showing extravascular deposition of fibrinogen, a sign of vessel leakage and irregularly shaped vasculature, these structures were reduced in tumors from tamoxifen-treated $CD4^{CreERT2}$ *Tgfbr2*$^{fl/fl}$PyMT mice (Extended Data Fig. 2a). In addition, the vessels in $CD4^{CreERT2}$ *Tgfbr2*$^{fl/fl}$PyMT tumors were surrounded by abundant $NG2^+$ pericytes and $GP38^+$ fibroblasts (Extended Data Fig. 2b), and ensheathed by highly connected basement membrane proteins collagen IV and fibronectin (Extended Data Fig. 2c). With this mature vasculature phenotype, there was a 6-fold increase of hypoxic areas adjacent to the dying tumor region (Extended Data Fig. 2d). Thus, the genetic blockage of TGF-β signaling in $CD4^+$ T cells is sufficient to trigger vasculature reorganization leading to tumor hypoxia and cancer cell death.

Our previous studies have shown that TGF-β1 produced by activated $CD4^+$ T cells, but not Treg cells or tumor cells, suppresses anti-tumor immunity[17-19], implying an autocrine

TGF-β Th cell control circuit in cancer immune evasion. To explore the pharmacologic blockade of TGF-β signaling in $CD4^+$ T cells, we employed protein-engineering techniques to generate bispecific antibodies, one specificity for CD4 and one for TGF-β. To achieve $CD4^+$ T cell targeting, we used ibalizumab, an anti-human CD4 (αCD4) that recognizes an epitope in the C2 domain of CD4 distinct from its major histocompatibility complex class II binding site[11,12]. The TGF-βRII extracellular domain (ECD) was utilized to block TGF-β signaling.

We engineered several bispecific formats with fusion of human TGF-βRII ECD to the antigen-binding (Fab) region of ibalizumab fused to a murine IgG1-Fc (fragment crystallized) where position 265 was mutated to alanine to prevent Fc receptor binding (Extended Data Fig. 3a). One of the formats with fusion of TGF-βRII ECD to the C-terminus of the antibody heavy chain, Fc-RIIECD, had high yield and low aggregation (Extended Data Fig. 3b-3c) and was chosen for further development as 'CD4 TGF-β Trap' (4T-Trap) (Fig. 2a). αCD4 and 4T-Trap, as well as a non-CD4-binding control antibody mGO53 and the mGO53 TGF-βRII ECD bispecifics (named as TGF-β-Trap), were expressed and purified to homogeneity (Fig. 2a and Extended Data Fig. 3d-3e). Binding of 4T-Trap and αCD4 to immobilized CD4 was similar with dissociation constants (Kd) around 0.1 nM (Fig. 2b and Extended Data Fig. 3f-3g), which was corroborated by their comparable binding to plasma membrane human CD4 ectopically expressed in HEK293 (293-hCD4) cells (Extended Data Fig. 3h). When compared to an anti-TGF-β (αTGF-β, 1D11 clone), 4T-Trap had a comparable association rate (Kon), but a faster dissociation rate (Koff) of binding to immobilized TGF-β1 (Fig. 2b and Extended Data Fig. 3g). However, in a TGF-β signaling reporter assay, 4T-Trap was a more effective inhibitor than αTGF-β showing 80% maximal inhibition (IC_{80}) at 1.3 nM and 25 nM, respectively (Extended Data Fig. 3i). Using enzyme-linked immunosorbent assays, CD4 binding for 4T-Trap versus αCD4 and TGF-β1 binding for 4T-Trap versus TGF-β-rap were comparable (Fig. 2c). Importantly, using a pretreatment scheme of incubation followed by washing, 4T-Trap, but not TGF-β-rap, inhibited TGF-β signaling in 293-hCD4 cells (Fig. 2d). These findings demonstrate that 4T-Trap preserves efficient CD4 binding and potent TGF-β signlaing inhibition properties.

The human CD4 epitope recognized by ibalizumab is not conserved in mice[11]. In order to test the therapeutic efficacy of 4T-Trap *in vivo*, we generated a strain of human CD4 transgenic (hCD4) mice using a bacterial artificial chromosome harboring the human *CD4* locus with the proximal enhancer region replaced by the murine equivalent to augment its expression[20] (Extended Data Fig. 4a). Flow cytometry experiments revealed exclusive expression of human CD4 on mouse $CD4^+$ T cells at a level comparable to that on human $CD4^+$ T cells (Extended Data Fig. 4b and data not shown). The *in vivo* pharmacokinectics (PK) of biotinylated 4T-Trap and control antibodies were assessed in hCD4 mice (Extended Data Fig. 5a). Following administration at a single dose of 150 μg, mGO53 and TGF-β-Trap showed a linear PK and long half-life ($t_{1/2}$ = 48 hr) in a 96 hr-testing window (Extended Data Fig. 5b). In contrast, αCD4 and 4T-Trap exhibited a nonlinear PK and short half-life ($t_{1/2}$ = 20 hr) irrespective of antibody doses (Extended Data Fig. 5b-5c), as a likely consequence of antibody internalization following CD4 binding. Accordingly, serum TGF-β1 was depleted by 4T-Trap and TGF-β-Trap, but not mGO53 or αCD4, and the depletion kinetics matched their respective PKs (Extended Data Fig. 5b and 5d).

Following administration to tumor-bearing hCD4PyMT mice, TGF-β-Trap and 4T-Trap substantially inhibited TGF-β signaling in cancer cells revealed by immunostaining of the phosphorylated Smad2 (pSmad2) (Extended Data Fig. 5e). pSmad2 was barely detectable by immunostaining in resting $CD4^+$ T cells from tumor-draining lymph nodes (data not shown), which was corroborated by comparable background flow cytometry signals in mice treated with all four groups of antibodies (Fig. 2e). Notably, T cell activation triggered substantial increase of pSmad2 in $CD4^+$ T cells from mGO53-, TGF-β-Trap- and αCD4-treated, but not 4T-Trap-treated mice (Fig. 2e), and the selective inhibitory activity of 4T-Trap versus TGF-β-Trap was associated with its targeting to $CD4^+$ T cells (Fig. 2f). In line with these observations, 4T-Trap target occupancy (TO) in $hCD4^+$ T cells approached 100% at 1 hr and 24 hr for all doses tested, which declined substantially at later time points (Extended data Fig. 5f). Notably, the 100 μg dose had an approximate 5% TO at 72 hr post-administration (Extended data Fig. 5f), which was sufficient to inhibit TGF-β signaling in $CD4^+$ T cells (Extended Data Fig. 5g). These findings reveal that although 4T-Trap and TGF-β-Trap are equally potent in neutralizing serum TGF-β1 and inhibiting TGF-β signaling in cancer cells, 4T-Trap is selectively delivered to lymph node $CD4^+$ T cells to potently suppress TGF-β signaling with a desirable pharmacodynamics (PD).

Based on the PK and PD properties of 4T-Trap, a treatment protocol of 100 μg/dose at twice a week was selected to explore its cancer therapeutic potential. hCD4PyMT mice bearing 5x5 mm tumors were treated with intravenous 4T-Trap or control antibodies including TGF-β-Trap, αCD4, and mGO53, for a total of 10 doses, and monitored for tumor growth for 6 weeks (Fig. 3a). Compared to control antibodies, 4T-Trap caused profound inhibition of tumor growth (Fig. 3b and Extended Data Fig. 5h). By immunohistological analyses, reorganized vasculature was only detected in the 4T-Trap group, manifested by reduced isolated $CD31^+$ staining (Extended Data Fig. 6a). Diminished extravascular deposition of fibrinogen was also observed (Extended Data Fig. 6a), suggesting that 4T-Trap treatment inhibited vasculature leakiness. To further interrogate the vasculature phenotype, we perfused mice with sulfo-NHS-biotin. Although vascular perfusion in tumors appeared heterogeneous and indistinguishable in all groups, much less extravascular biotinylation of cancer cells was observed in the 4T-Trap group (Extended Data Fig. 6b), corroborating the nonporous vasculature phenotype. The vascular functionality change was associated with alteration of the vascular structure manifested by the tightly enwrapped $NG2^+$ pericytes and $GP38^+$ fibroblasts as well as the highly connected basement membrane proteins collagen IV and fibronectin in the 4T-Trap group (Extended Data Fig. 6c-6d). These findings demonstrate that 4T-Trap is efficacious in promoting vasculature reorganization and cancer suppression.

To better characterize the therapeutic effects of 4T-Trap, we monitored tumor vasculature dynamics and cancer cell fates in hCD4PyMT mice treated with 4T-Trap or control antibodies. At 1~2 weeks posttreatment, comparable sprouting angiogenesis in the tumor parenchyma was observed in all groups of mice (Fig. 3c). At 3~4 weeks, while vessel density was unchanged, the number of isolated $CD31^+$ staining was increased in mice treated with mGO53, TGF-β-rap, or αCD4 control antibodies (Fig. 3c). In contrast, the bluntly ended blood vasculature was substantially repressed in mice treated with 4T-Trap (Fig. 3c), associated with an approximate 30-fold increase of hypoxic areas with minimal

cancer cell death (Fig. 3c). By 5~6 weeks, the irregularly shaped blood vasculature was much more exaggerated in all control groups (Fig. 3c), but was further suppressed in 4T-Trap-treated mice (Fig. 3c), triggering catastrophic cancer cell death in hypoxic areas distant to the vasculature (Fig. 3c). Similar 4T-Trap-triggered tumor growth, vasculature remodeling and cancer cell death phenotypes were observed in mice bearing more advanced 9x9 mm tumors (Extended Data Fig. 7a-7c). These findings suggest that 4T-Trap restrains tumor progression by the induction of vasculature pruning and reorganization, which results in hypoxia and starvation-triggered cancer cell death.

4T-Trap treatment led to increased proportions of effector/memory $CD4^+$ T cells in the tumor-draining lymph nodes (Extended Data Fig. 8a), which was associated with diminished expression of TGF-β target genes *Smad7* and *Rgs16* (Extended Data Fig. 8b). Furthermore, 4T-Trap treatment resulted in enhanced differentiation of IFN-β-producing Th1 and IL-4-producing Th2 cells as well as increased tumor infiltration of conventional $CD4^+Foxp3^-$ T cells at the expense of $CD8^+$ T cells (Extended Data Fig. 8c-8d). Notably, neutralization of IL-4, but not IFN-γ, reversed the tumor suppression phenotype (Extended Data Fig. 9a-9b), which was associated with attenuated vessel reorganization, diminished hypoxia, and reduced cancer cell death (Extended Data Fig. 9c). To extend these studies to other cancer models, hCD4 mice were subcutaneously inoculated with MC38 cells, followed by treatment with either 4T-Trap or control antibodies (Extended Data Fig. 9d). We observed selective suppression of tumor growth in 4T-Trap-treated mice (Extended Data Fig. 9e). Neutralization of IL-4 fully reversed the tumor repression phenotype (Extended Data Fig. 9f), while partial effect was observed with an IFN-γ blockade (Extended Data Fig. 9g).

Hypoxia triggers cellular adaptation to resolve ischemia via the induction of angiogenic factors such as VEGFA[21]. Indeed, while low level VEGFA expression was observed in tumors from hCD4PyMT mice treated with control antibodies (Fig. 4a), enhanced VEGFA expression in hypoxic areas was detected in mice treated with 4T-Trap (Fig. 4a). To investigate the functional significance of such an adaptive response, we engineered a VEGF receptor decoy called VEGF-Trap, wherein fragments of VEGF receptors[22] were fused to a murine IgG2a-Fc (Extended Data Fig. 7d-7e). Compared to mGO53 control, VEGF-Trap treatment diminished tumor vessel density, but did not affect vessel patterning, and negligible effects on tumor tissue oxygenation or cancer cell survival were observed (Fig. 4b). Notably, co-administration of VEGF-Trap with 4T-Trap resulted in low vessel density in addition to its reorganization (Fig. 4b), which expanded cancer cell death regions at the expense of hypoxic areas (Fig. 4b), as a likely consequence of more severe nutrient deprivation in regions of hypoxia. In fact, while a hypoxic zone at the periphery of the cancer cell death region was detected in 4T-Trap-treated mice, with 4T-Trap plus VEGF-Trap treatment, the cancer cell death region expanded to the outer boundary of hypoxic areas (Fig. 4c). Importantly, while VEGF-Trap had no impact on tumor growth or survival of hCD4PyMT mice in line with previous studies[10] (Fig. 4d-4e), it enhanced the tumor suppression and survival benefits of 4T-Trap (Fig. 4d-4e). These findings demonstrate that 4T-Trap can be combined with VEGF inhibitors to further restrain the tumor vasculature-mediated cancer progression.

TGF-β is a multifunctional cytokine with pleiotropic roles in diverse pathophysiological processes, rendering the approach of general TGF-β inhibition for cancer therapy an enormous challenge[23-26]. Herein, we found that targeted TGF-β signaling inhibition in $CD4^+$ T cells revives helper T cell responses and suppresses cancer progression, a process mediated by the induction of vasculature reorganization with hypoxia and cancer cell death being secondary outcomes. Such a host-centric cancer defense response is dependent on IL-4. Future studies will clarify whether the type 2 immunity represents a general anti-cancer mechanism, or if the 4T-Trap-elicited type 1 immune response can also be harnessed to suppress tumor development as suggested by recent studies[27-29]. Notably, while VEGF-Trap induces quantitative vasculature change, 4T-Trap triggers qualitative vasculature remodeling. These findings raise the possibility that immunological mechanisms of vessel reprogramming may underscore the master plan of cancer environment-directed therapies (Extended Data Fig. 10). Further development of 4T-Trap and its testing in the clinic should provide further opportunities to exploit this tissue-level cancer immunotherapy approach.

Methods

Mice.

CD4^{CreERT2} mice were purchased from the Jackson Laboratory. *Tgfbr2*$^{fl/fl}$ and MMTV-PyMT (PyMT) mice were maintained in the laboratory as previously described[31,32]. The human CD4 (hCD4) transgenic mice were generated by pronuclear microinjection of fertilized eggs with a modified bacterial artificial chromosome (BAC) containing the human *CD4* gene locus with the proximal enhancer region replaced by its murine equivalent. Briefly, a BAC harboring the human *CD4* gene locus was recombineered with a pLD53.SC-AB shuttle plasmid containing the mouse *Cd4* proximal enhancer[33] flanked by two homologous arms of the human *CD4* gene. Founder hCD4 mouse strains were screened by PCR with human *CD4*-specific primers. All mice were backcrossed to the C57BL/6J background, and maintained under specific pathogen-free conditions. Animal experimentation was conducted in accordance with procedures approved by the Institutional Animal Care and Use Committee of Memorial Sloan Kettering Cancer Center.

Tumor measurement.

Mammary tumors in female PyMT mice or transplanted MC38 tumors were measured weekly with a caliper. Tumor burden was calculated using the equation $[(LxW^2) \times (\pi/6)]$, in which L and W denote length and width. Total tumor burden was calculated by summing up individual tumor volumes of each mouse with an end-point defined when total burden reached 3,000 mm^3 or one tumor reached 2,000 mm^3.

Therapeutic treatment.

For TGF-βRII inducible deletion tumor model, *Tgfbr2*$^{fl/fl}$PyMT and CD4^{CreERT2}*Tgfbr2*$^{fl/fl}$PyMT mice bearing 5x5 - 6x6 mm (LxW) tumors were left untreated or treated with 100 μL tamoxifen (Sigma) dissolved in corn oil at 50 mg/mL by oral gavage twice a week for 6 weeks. For small tumor treatment, hCD4PyMT mice harboring 5x5 mm tumors were intravenously injected twice a week for 5 weeks with mGO53 (100 μg), TGF-β-rap (100 μg), αCD4 (100 μg), 4T-Trap (100 μg) or combination of αCD4 (100

μg) with TGF-β-rap (100 μg) in 0.1-0.2 mL PBS. For larger tumor treatment, hCD4PyMT mice harboring 9x9 mm tumors were intravenously injected twice a week for 4 weeks with mGO53 (100 μg), TGF-β-rap (100 μg), αCD4 (100 μg) or 4T-Trap (100 μg) in 0.1 mL PBS. For IL-4 and IFN-γ neutralization experiments, hCD4PyMT mice harboring 5x5 mm tumors or hCD4 mice transplanted with MC38 tumor cell lines were intravenously injected twice a week with mGO53 (200 μg), 4T-Trap (100 μg) + mGO53 (100 μg), αIL-4 (100 μg) + mGO53 (100 μg), αIFN-γ (100 μg) + mGO53 (100 μg), 4T-Trap (100 μg) + αIFN-4 (100 μg) or 4T-Trap (100 μg) + αIFN-γ (100 μg) in 0.2 mL PBS. To assess 4T-Trap performance versus VEGF-Trap, hCD4PyMT mice harboring 5x5 mm tumors were intravenously injected twice a week for 5 weeks with mGO53 (200 μg), VEGF-Trap (100 μg) + mGO53 (100 μg), 4T-Trap (100 μg) + mGO53 (100 μg) or 4T-Trap (100 μg) + VEGF-Trap (100 μg) in 0.2 mL PBS. The IL-4 neutralizing antibody (11D11) and IFN-γ neutralizing antibody (XMG1.2) were purchased from Bio X Cell.

Immune cell isolation from tissues.

Single-cell suspensions were prepared from lymph nodes and spleens by tissue disruption with glass slides. The dissociated cells were passed through 70 μm filters and pelleted. Tumor-infiltrating immune cells were isolated from mammary tumors as previously described[34]. Briefly, tumor tissues were minced with a razor blade then digested in 280 U/mL Collagenase Type 3 (Worthington Biochemical) and 4 μg/mL DNase I (Sigma) in HBSS at 37°C for 1 hr and 15 min with periodic vortex every 20 min. Digested tissues were passed through 70 μm filters and pelleted. Cells were resuspended in 40% Percoll (Sigma) and layered above 60% Percoll. Sample was centrifuged at 1,900 g at 4°C for 30 min without brake. Cells at interface were collected, stained and analyzed by flow cytometry.

Flow cytometry.

Flurochrome-conjugated or biotinylated antibodies against mouse CD4 (RM4-5), CD8 (53-6.7), Foxp3 (FJK-16s), IFN-γ (XMG1.2), IL-4 (BVD6-24G2), NK1.1 (PK136), TCRβ (H57-595), CD45 (30-F11), CD44 (IM7), CD62L (MEL-14), CD11b (M1/70), B220 (RA3-6B2), XCR1 (ZET), NKp46 (29A1.4), CD11c (N418), Ly6c (AL-21), Ly6G (1A8), MHC-II I-A/I-E (M5/114.15.2) were purchased from BD Biosciences, TonBo, eBioscience, Invitrogen and BioLegend. All antibodies were tested with their respective isotype controls. Cell-surface staining was conducted by incubating cells with antibodies for 30 min on ice in the presence of 2.4G2 mAb to block FcγR binding. For Foxp3 staining, a transcription factor-staining kit (Tonbo Biosciences) was used. To assess cytokine production, T cells were stimulated with 50 ng/mL phorbol 12-myristate 13-acetate (Sigma), 1 mM ionomycin (Sigma) in the presence of Golgi-Stop (BD Biosciences) for 4 hr at 37°C as previously described[35]. T cells were subsequently stained for cell surface markers before intracellular cytokine staining. All data were acquired using an LSRII flow cytometer (Becton Dickinson) and analyzed with FlowJo software (Tree Star, Inc.).

Immunofluorescence staining.

Antibodies against CD31 (MEC13.3) and GP38 (8.1.1) were purchased from Biolegend. Antibodies against Col IV (Cat. #2150-1470) and fibrinogen (Cat. #4440-8004) were obtained from Bio-rad. Antibodies against fibronectin (Cat. #AB2033), NG2 (Cat.

#AB5320) and cleaved caspase 3 (Cat. #9661S) and phosphorylated Smad2 (Cat. #3108S) were purchased from EMD and Cell Signaling Technology, respectively. Antibodies against E-Cadherin (DECMA-1) and Ki67 (SolA15) were obtained from eBioscience. Antibody against VEGFA (Cat. #AF-493-NA) was purchased from R&D Systems. Tumor tissues were frozen in O.C.T. medium (Sakura Finetek USA) and sectioned at the thickness of 10 μm. Tumor sections were fixed and stained with antibodies. Subsequently, they were mounted with VECTORSHIELD anti-fade mounting media (Vector Laboratories) and scanned by Pannoramic Digital Slide Scanners (3DHISTECH LTD). Immunofluorescence images were analyzed with CaseViewer and Fiji software, and further processed in Adobe photoshop and Illustrator software. To assess hypoxia response, 60 mg/kg pimonidazole hydrochloride was administered to mice via intraperitoneal injection. 1 h later, mice were sacrificed and tumor tissues were harvested. To detect the formation of pimonidazole adducts, tumor cryosections were immunostained with a Hypoxyprobe kit (Hypoxyprobe, Inc.) following the manufacturer's instructions. For sulfo-NHS-biotin perfusion, deeply anesthetized mice were perfused with 20-mL 0.3 mg/mL sulfo-NHS-Biotin (Thermo Scientific) in PBS, followed by 2% PFA in PBS. Tumor sections were incubated with FITC streptavidin (Biolegend) diluted in PBST.

Cell lines.

HEK293 cells (Cat. #CRL-1573) and 1D11.16.8 hybridoma cell lines (Cat. #HB-9849) were purchased from ATCC. FreeStyle 293-F cells (Cat. #K9000-01) were obtained from ThermoFisher Scientific. Sf9 and Hi5 insect cell lines were kind gifts from Prof. Morgan Huse (MSKCC). MC38 colon cancer cell line was a kind gift from Prof. Jedd Wolchok (MSKCC). HEK293 cells stably expressing human CD4 were generated by retrovirus-mediated gene transfer. Briefly, HEK293 cells (5×10^6) plated on 10 cm dishes were transfected with a human CD4-expressing retroviral vector containing an EGFP reporter (10 μg) together with a helper plasmid (5 μg). Two days after transfection, the viruses were harvested and used to infect HEK293 cells in the presence of 4 μg/mL polybrene (Sigma). Infection was repeated twice to enhance the transduction efficiency, and cells were selected by flow cytometry sorting based on EGFP signals.

Antibody cloning.

DNA fragments of the ibalizumab VH domain were synthesized by Genewiz. Antibody protein fusion constructs were generated by overlapping PCR of DNA fragments encoding the ibalizumab or mGO53 VH domain and a mouse IgG1 constant region domain. To abrogate IgG1 Fc effector functions, a D265A mutation was introduced by site-directed mutagenesis (Agilent Technologies). A DNA fragment encoding the human TGF-βRII extracellular domain (ECD) was chemically synthesized (Genewiz), and fused to antibody expression constructs via a DNA fragment encoding a $(Gly_3Ser)_3$ linker. The VEGF-Trap expressing construct was created by overlapping PCR of DNA fragments encoding a mouse IgG2a Fc domain, the second Ig domain of human VEGFR1 and the third Ig domain of human VEGFR2 as previously described[36].

Antibody expression and purification.

Antibody-encoding plasmids were transiently transfected into FreeStyle 293-F cell lines. Cell culture supernatants were collected 4 days post-transfection, cleared by low-speed centrifugation and 0.45 μm filters, diluted with a 10x binding buffer (0.2 M Na_3PO_4, pH 7.0) and passed through a protein A/G prepackaged gravity flow column (GE Healthcare). Antibodies were eluted with 0.1 M glycine-HCl (pH 2.7) into a neutralizing buffer (1 M Tris-HCl, pH 9.0), concentrated by centrifugation and buffer-exchanged into PBS (pH 7.4). Antibodies were quantified by spectrophotometry, and their purities were assessed by electrophoresis followed by Coomassie Blue staining. Size exclusion chromatography was used to further assess physicochemical homogeneity of antibodies and to resolve monomers from non-monomeric species. Briefly, antibodies were passed through an AKTA purifier (GE Healthcare) on a Superdex S200 10/300 GL column (GE Healthcare) with a mobile phase of PBS at a flow rate of 0.5 mL/min. Percent monomer was calculated as the area of the monomeric peak divided by the total area of monomeric plus nonmonomeric peaks at 280 nm. Antibody solutions were filtered through 0.22 μm filterers, validated for low endotoxin levels using a LAL chromogenic endotoxin quantification kit (Thermo Scientific) before used for experiments. To biotinylate antibodies, the C-terminus of antibody light chain was fused with a biotin-binding peptide, and subjected for *in vitro* biotinylation with a BirA biotin-protein ligase reaction kit (Avidity).

Recombinant CD4 expression and purification.

A DNA fragment encoding the extracellular domain of human CD4 (residues 26-390) with N-terminal fusion of the gp67 secretion signal and C-terminal fusion of a His tag was cloned into the baculovirus expression vector pAcGP67-A (BD Biosciences). Recombinant baculovirus was packaged in Sf9 cells, and used to infect Hi5 cells for CD4 protein expression. In a typical preparation, 500 mL liquid culture of Hi5 cells at a concentration of $2x10^6$ cells/mL were inoculated with 12 mL recombinant baculovirus at a concentration of $2x10^8$ pfu/mL. Supernatants were harvested 2 days after infection, and loaded onto a Ni^{2+}-NTA column (GE Healthcare) for affinity purification. Recombinant CD4 was further purified by sequential Superdex S-75 and MonoQ columns.

Surface plasmon resonance.

Binding affinity analyses of 4T-Trap, αCD4 and an anti-TGF-β αTGF-β, 1D11 clone purified from 1D11.16.8 hybridoma cell line) were performed with a previously described protocol[37]. Briefly, recombinant human CD4 or TGF-β1 (Cat. #240-B-010, R&D systems) was immobilized to CM5 sensor chips. The binding kinetics was monitored by flowing 4T-Trap, αCD4 and αTGF-β over the chip for association, which was further monitored for their dissociation with the surface being washed for 5 min.

4T-Trap binding to cell surface CD4.

Serial dilutions of 4T-Trap or αCD4 were prepared in 96-well U-bottom plates in DMEM medium. $2x10^5$ HEK293-hCD4 cells were added to each well and incubated on ice for 1 hr with shaking every 10 min. Cells were washed, resuspended and incubated in PE-conjugated donkey anti-mouse IgG (Cat. #12-4012-82, eBioscience) on ice for 30 min with shaking

every 10 min. Cells were rewashed and analyzed by flow cytometry. The mean fluorescence intensity value was quantified.

Enzyme-Linked Immunosorbent Assay (ELISA).

Costar 96-well ELISA plates (Corning) were coated with 50 ng recombinant human CD4 or TGF-β1 for 18 hr at 4°C. Plates were washed four times with 0.05% Tween-20 in PBS and blocked with 0.5% BSA in PBS for 1 hr at room temperature. Serial dilutions of 4T-Trap or control antibodies were plated in triplicates and incubated at room temperature for 2 hr. Plates were washed four times and incubated with peroxidase-conjugated goat anti-mouse IgG (Cat. #115-035-003, Jackson Immuno Research) at 37°C for 1 hr. To detect CD4 and TGF-β1 co-binding, CD4-coated plates that had been incubated with 4T-Trap or control antibodies were incubated with 100 ng recombinant TGF-β1 for 2 hr. Plates were washed and incubated with a biotinylated TGF-β1 antibody (Cat. # BAF240, R&D systems) at room temperature for 2 hr. Plates were further washed and incubated with peroxidase-conjugated streptavidin (Jackson Immuno Research) at 37°C for 1 hr. After final washes, plates were incubated in a TMB solution at room temperature for 5 to 20 min, and the reaction was terminated with 1 M HCl. Plate absorbance at 450 nm with background correction at 570 nm was detected with a SpectraMax 384 Plus Microplate Reader (Molecular Devices).

Pharmacokinetic analysis and serum TGF-β1 measurement.

Plasma samples were drawn from hCD4 transgenic mice after intravenous injection of biotinylated 4T-Trap or control antibodies for 1, 24, 48, 72 and 96 hr. Streptavidin-coated plates (ThermoFisher Scientific) were incubated with plasma samples and standards at 37°C for 1 hr, washed four times and incubated with peroxidase-conjugated goat anti-mouse IgG at 37°C for 1 hr. As for serum TGF-β1 level measurement, costar 96-well ELISA plates coated with 1 μg αTGF-β (1D11) antibody for 18 hr at 4°C, were incubated with plasma samples (pretreated with hydrochloric acid) and standards at 37°C for 1 hr, washed four times and incubated with a biotinylated TGF-β1 antibody (Cat. # BAF240, R&D systems) at room temperature for 2 hr. Plates were further washed and incubated with peroxidase-conjugated streptavidin (Jackson Immuno Research) at 37°C for 1 hr. After final washes, plates were incubated in a TMB solution at room temperature for 5 to 20 min and the reaction was terminated with 1 M HCl. Plate absorbance at 450 nm with a background correction at 570 nm was detected in a SpectraMax 384 Plus Microplate Reader (Molecular Devices).

Luciferase reporter assays.

To assess TGF-β signaling, HEK293 cells or HEK293-hCD4 cells transfected with a TGF-β/SMAD Firefly luciferase reporter plasmid[38] and a pRL-TK Renilla luciferase reporter plasmid were plated in 24-well plates at $2x10^5$ cells per well in 500 μL of DMEM medium, and cultured for 18 hr at 37°C. Plates were subsequently incubated with serial dilutions of 4T-Trap or control antibodies in DMEM medium for 30 min, which were left unwashed or washed and re-cultured with 10 ng/mL recombinant human TGF-β1 in DMEM medium for 12 hr. Cells were subsequently lysed, and assyaed for luciferase activities with a dual-specific luciferase reporter assay system (Promega). To validate VEGF-Trap inhibition of VEGF signaling, HEK293 cells were co-transfected with a VEGF-responsive

NFAT Firefly luciferase reporter plasmid[39], a VEGFR2 expression plasmid and a pRL-TK Renilla luciferase reporter plasmid. Plates were subsequently incubated with serial dilutions of VEGF-Trap and 10 ng/mL recombinant mouse $VEGF_{165}$ (Cat. # 450-32, Peprotech) for 12 hr before luciferase activities were measured.

Immunoblotting.

$CD4^+$ T cells from hCD4 transgenic mice were purified using a Magnisort Mouse CD4 T Cell Enrichment Kit (Affymetrix), and incubated with 10 ng/mL, 50 ng/mL, 100 ng/mL or 500 ng/mL 4T-Trap for 10 min. Cells were washed, cultured with 10 ng/mL recombinant human TGF-β1 for 1 hr, and collected into a cell lysis buffer (50 mM Tris-HCl, pH 7.6, 150 mM NaCl, 0.5% Triton-X-100, 2mM EGTA, 10 mM NaF, 1mM Na_3VO_4 and 2 mM DTT) supplemented with protease inhibitors. Protein extracts were made, separated by SDS-PAGE gel and blotted with SMAD2/3 (D7G7) and phospho-SMAD2(Ser465/467)/SMAD3(S423/S425) (D27F4) antibodies from Cell Signaling Technology.

Quantitative RT-PCR.

Effector/memory $CD4^+$ T cells from tumor-draining lymph nodes were isolated with an EasySep Mouse Memory $CD4^+$ T cell Isolation Kit (STEMCELL). Total RNA was extracted with an RNeasy Micro Kit (Qiagen), reversed-transcribed with SuperScript II Reverse Transcriptase (ThermoFisher), and amplified in a StepOnePlus Real-Time PCR System with SYBR Green PCR Master Mix (Applied Biosystems). The change-in-cycling-threshold ($2^{-\Delta\Delta Ct}$) method was used for calculation of relative target gene expression normalized to the housekeeping transcript *Gapdh*. RT-PCR primer pairs included *Smad7* Forward: ggaagatcaaccccgagctg; Reverse: cagcctgcagttggtttgaga; *Rgs16*, Forward: tgccactaccagttgcttcg; Reverse: cttgaggaagcgcggatagg; *Gapdh*, Forward: 5'-atggtgaaggtcggtgtgaa-3'; Reverse: 5'-cgctcctggaagatggtgat-3'.

CD4 target occupancy assay.

100 μL blood was collected retro-orbitally in EDTA-coated Eppendorf tubes from mice that had been intravenously administered with biotinylated 4T-Trap. The blood samples were divided into two groups. The first group was spiked with 1 μg biotinylated 4T-Trap for 30 min at 4°C as a 100% target occupancy (TO) control, while the second group was left untreated. All samples were washed twice with 1% FBS in PBS and stained with PE-conjugated streptavidin and a cocktail of antibodies against T cell surface markers for 30 min at 4°C. Cells were re-washed and analyzed by flow cytometry. The TO percentage was calculated as 100 x [Mean Fluorescence Intensity (MFI) of sample PE signal/MFI of spiked sample PE signal].

Statistical analysis.

All experiments were repeated at least three times except measurements of individual tumors. All statistical measurements are displayed as mean ± SEM. For comparisons of two groups, unpaired Student's *t*-test (two-tailed) was conducted. For paired distance comparisons, paired *t*-test (two-tailed) was conducted. For comparisons of more than two groups, data were analyzed by one-way ANOVA and results were adjusted with the

Bonferroni's correction. For multiple group comparisons with more than one independent variable, two-way ANOVA was used. Data were analyzed with GraphPad Prism Software. Fluorescent-imaging analysis was performed in a blinded fashion.

Reporting Summary

Further information on research design is available in the Nature Research Reporting Summary linked to this paper.

Extended Data

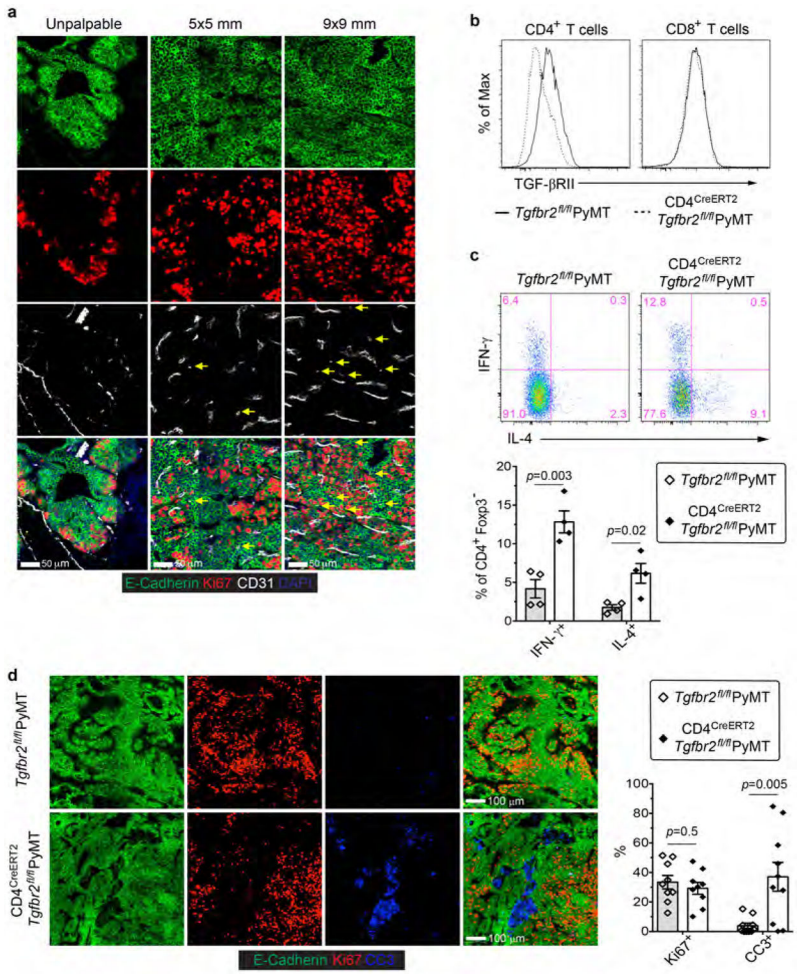

Extended Data Fig. 1 |. Inducible ablation of TGF-βRII in CD4$^+$ T cells causes enhanced T helper cell responses and increased cancer cell death.

a, Representative immunofluorescence images of CD31 (white), Ki67 (red) and E-Cadherin (green) in mammary tumor tissues from PyMT mice harboring unpalpable, 5x5 mm, or 9x9 mm tumors. Isolated CD31$^+$ staining in the tumor parenchyma (yellow arrows) is indicated. **b,** TGF-βRII expression on CD4$^+$ T cells and CD8$^+$ T cells from the tumor-draining lymph nodes of *Tgfbr2*$^{fl/fl}$PyMT and CD4^{CreERT2} *Tgfbr2*$^{fl/fl}$PyMT mice treated with tamoxifen. **c,** Representative flow cytometry plots and statistical analyses

of IL-4 and IFN-γ expression in $CD4^+Foxp3^-$ T cells from the tumor-draining lymph nodes of *Tgfbr2*$^{fl/fl}$PyMT and $CD4^{CreERT2}$*Tgfbr2*$^{fl/fl}$PyMT mice treated with tamoxifen. **d**, Representative immunofluorescence images of E-Cadherin (green), Ki67 (red) and cleaved Caspase 3 (CC3, blue) in mammary tumor tissues from *Tgfbr2*$^{fl/fl}$PyMT and $CD4^{CreERT2}$*Tgfbr2*$^{fl/fl}$PyMT mice treated with tamoxifen. The percentage of $Ki67^+$E-$Cadherin^+$ cells over total E-$Cadherin^+$ epithelial cells was calculated from 0.02 mm^2 regions (n=9). The percentage of $CC3^+$ areas over total E-$Cadherin^+$ areas was calculated from 0.02 mm^2 regions (n=10). All statistical data are shown as mean ± SEM. Two-tailed unpaired *t*-test (**c**, **d**). Data are pooled biological replicates (**c**) or representative of three independent experiments (**a**, **b**, **d**).

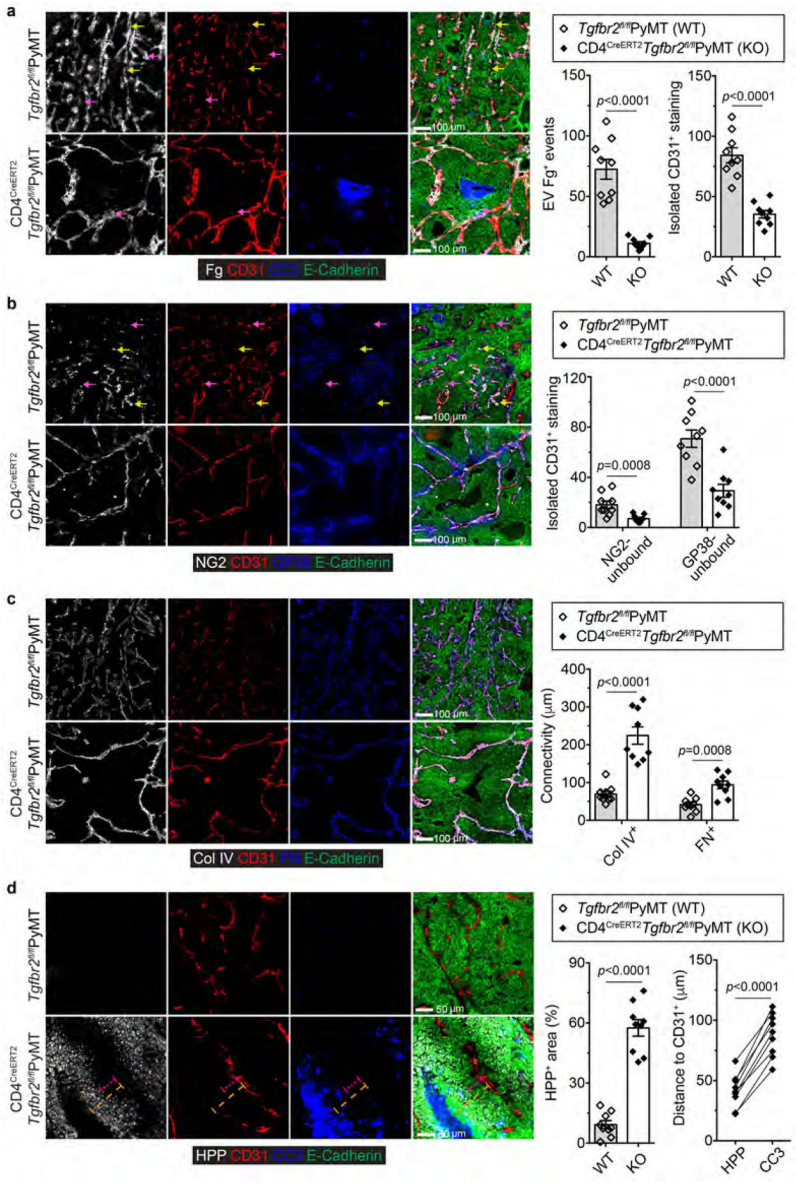

Extended Data Fig. 2 |. Inducible ablation of TGF-βRII in $CD4^+$ T cells promotes tumor vessel reorganization, hypoxia and cancer cell death.

a, Representative immunofluorescence images of fibrinogen (Fg, white), CD31 (red), cleaved Caspase 3 (CC3, cyan) and E-Cadherin (green) in mammary tumor tissues from *Tgfbr2*$^{fl/fl}$PyMT and CD4^{CreERT2} *Tgfbr2*$^{fl/fl}$PyMT mice treated with tamoxifen. Extravascular (EV) Fg deposition events (magenta arrows) were calculated from 1 mm^2 regions (n=9 for each group). Isolated CD31$^+$ staining (yellow arrows) was counted from 1 mm^2 regions (n=9 for each group). **b,** Representative immunofluorescence images of NG2$^+$ pericytes (white), CD31$^+$ endothelial cells (red), GP38$^+$ fibroblasts (blue) and E-Cadherin (green) in mammary tumor tissues from *Tgfbr2*$^{fl/fl}$PyMT and CD4^{CreERT2} *Tgfbr2*$^{fl/fl}$PyMT mice treated with tamoxifen. NG2-unbound (magenta arrows) or GP38-unbound (yellow arrows) isolated CD31$^+$ staining was counted from 1 mm^2 regions (n=9 for each group). **c,** Representative immunofluorescence images of collagen IV (Col IV, white), CD31 (red), fibronectin (FN, cyan) and E-Cadherin (green) in mammary tumor tissues from *Tgfbr2*$^{fl/fl}$PyMT and CD4^{CreERT2} *Tgfbr2*$^{fl/fl}$PyMT mice treated with tamoxifen. The average continuous lengths of Col IV and FN were measured in 1 mm^2 regions (n=9 for each group). **d,** Representative immunofluorescence images of a hypoxia probe (HPP, white), CD31 (red), CC3 (cyan) and E-Cadherin (green) in mammary tumor tissues from *Tgfbr2*$^{fl/fl}$PyMT and CD4^{CreERT2} *Tgfbr2*$^{fl/fl}$PyMT mice treated with tamoxifen. The percentage of HPP$^+$E-Cadherin$^+$ areas over E-Cadherin$^+$ epithelial areas was calculated from 1 mm^2 regions (n=9 for each group). The shortest distance of HPP$^+$ regions (magenta dashed lines) or CC3$^+$ regions (yellow dashed lines) to CD31$^+$ endothelial cells was measured in tumor tissues from CD4^{CreERT2} *Tgfbr2*$^{fl/fl}$PyMT mice treated with tamoxifen (n=9). All statistical data are shown as mean ± SEM. Two-tailed unpaired *t*-test (**a-d**) or paired *t*-test (**d**). Data are representative of three independent experiments (**a-d**).

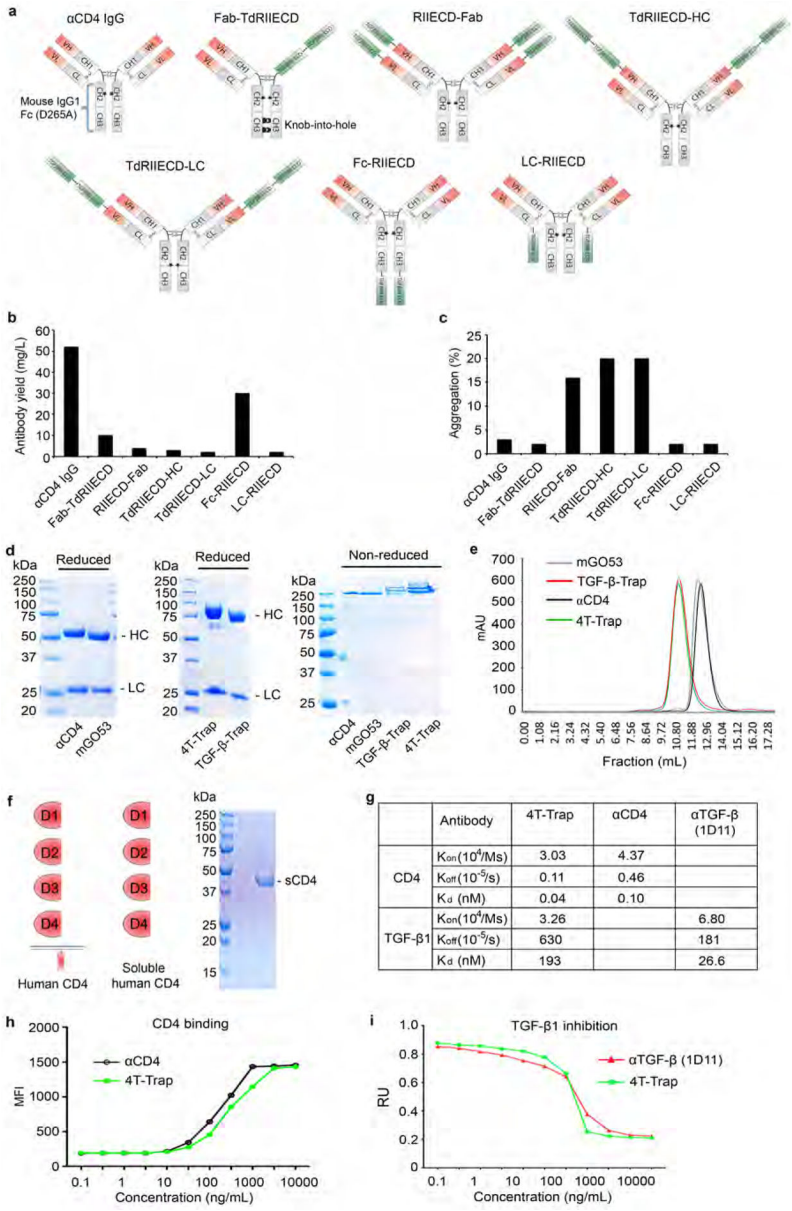

	Antibody	4T-Trap	αCD4	αTGF-β (1D11)
CD4	K_{on}(10^4/Ms)	3.03	4.37	
	K_{off}(10^{-5}/s)	0.11	0.46	
	K_d (nM)	0.04	0.10	
TGF-β1	K_{on}(10^4/Ms)	3.26		6.80
	K_{off}(10^{-5}/s)	630		181
	K_d (nM)	193		26.6

Extended Data Fig. 3 |. Biochemical properties of 4T-Trap and control antibodies.

a, Schematic representation of ibalizumab Fab and TGF-βRII ECD fusion proteins in a murine IgG1 framework. The star indicates a D265A substitution in the CH2 domain, and the semicircle and moon shapes indicate knob-into-hole (KIH) modifications in the CH3 domain to enable heavy chain heterodimerization. The gray or colored parts indicate mouse or human sequences, respectively. **b-c**, Yield and aggregation percentage of ibalizumab Fab and TGF-βRII ECD fusion proteins produced in a FreeStyle HEK293-F cell transient expression system. FreeStyle HEK293-F cells transfected with plasmids encoding the indicated fusion antibodies were cultured for 4 days, and the supernatant was collected. Protein G affinity purification and size exclusion chromatography were used to purify these antibodies. **d**, Molecular weights of αCD4, mGO53, 4T-Trap and TGF-β-Trap antibodies detected by Coomassie Blue staining of samples run in a SDS-PAGE gel under non-reduced

or reduced conditions. Molecular size markers (kDa) are shown on the left. HC, heavy chain; LC, light chain. **e**, Size exclusion chromatography analyses of mGO53, TGF-β-Trap, αCD4 and 4T-Trap antibodies. **f**, Schematic representation of human CD4 structure and purity examination of recombinant soluble CD4 (sCD4) by SDS-PAGE followed Coomassie Blue staining. **g**, The binding affinities of 4T-Trap and αCD4 to human CD4 as well as 4T-Trap and αTGF-β (1D11 clone) to human TGF-β1 were determined by surface plasmon resonance. **h**, Binding of 4T-Trap to human CD4 ectopically expressed on HEK293 cells. Cells were incubated with serial dilutions of 4T-Trap and αCD4 antibodies followed by a fluorophore-conjugated anti-mouse IgG secondary antibody. Samples were analyzed by flow cytometry. The measured mean fluorescence intensity (MFI) was quantified. **i**, TGF-β signaling inhibitory functions of 4T-Trap and αTGF-β. HEK293 cells transfected with a TGF-β/SMAD firefly luciferase reporter plasmid and a pRL-TK Renilla luciferase reporter plasmid were incubated with the indicated antibodies for 30 min and treated with 10 ng/mL recombinant human TGF-β1 for 12 hr before subject to the luciferase assay. RU, relative unit of normalized Firefly luciferase activity to Renilla luciferase activity. Data are representative of three independent experiments (**b**-**f**, **h**, **i**).

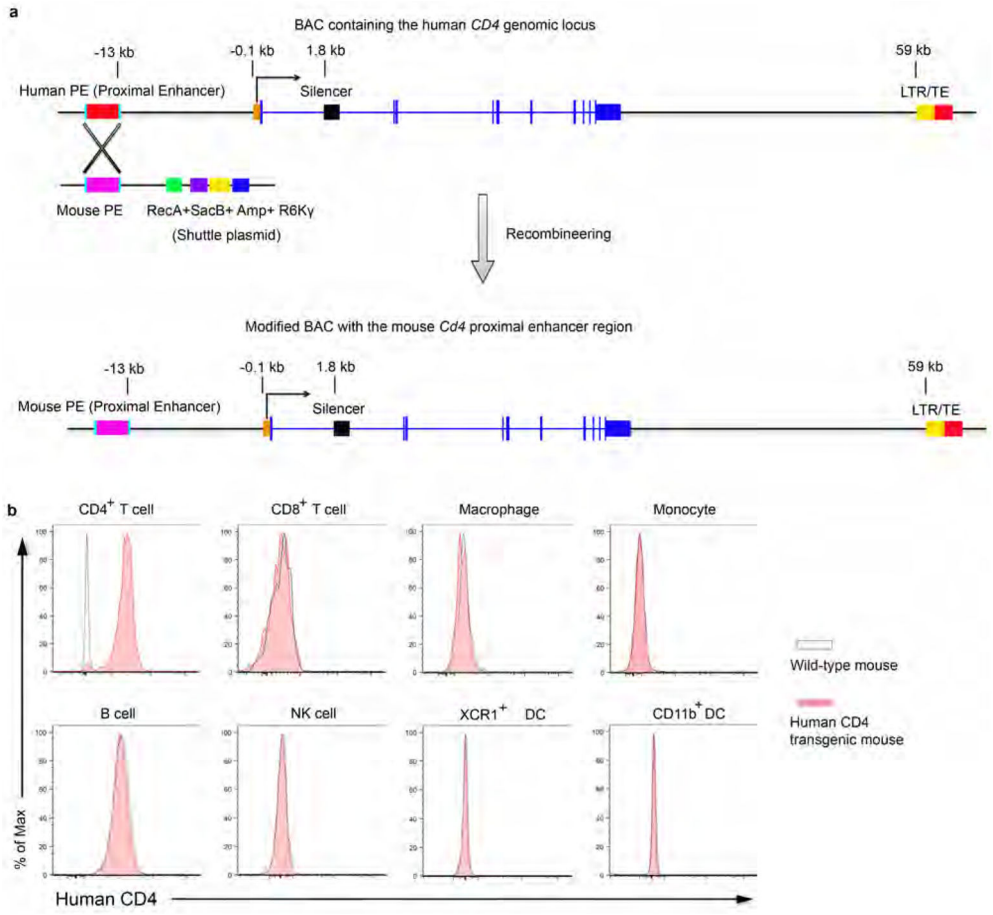

Extended Data Fig. 4 |. Generation and validation of human CD4 transgenic mice.
a, Recombineering a bacterial artificial chromosome (BAC) DNA containing the human *CD4* locus with the proximal enhancer (PE) element replaced by its murine equivalent.

The shuttle plasmid contains the mouse *Cd4* PE flanked by two homologous arms of the human *CD4* gene (250 bps), the E coli. *RecA* gene to mediate homologous recombination, the *SacB* gene to mediate negative selection on sucrose, an Ampicillin resistance locus to mediate positive selection and a conditional R6Kγ replication origin. **b**, Flow cytometry analyses of human CD4 expression on leukocyte populations from wild-type or human CD4 transgenic mice. $CD4^+$ T cells ($CD45^+TCR\beta^+CD4^+$), $CD8^+$ T cells ($CD45^+TCR\beta^+CD8^+$), NK cells ($CD45^+TCR\gamma^-TCR\beta^-NKp46^+NK1.1^+$) were isolated from lymph nodes. B cells ($CD45^+MHCII^+Ly6C^-B220^+$), $XCR1^+$ dendritic cells (DCs) ($CD45^+Lin^-F4/80^-Ly6C^-CD11c^+MHCII^+XCR1^+$), $CD11b^+$ DCs ($CD45^+Lin^-F4/80^-Ly6C^-CD11c^+MHCII^+CD11b^+$), Monocytes ($CD45^+Lin^-F4/80^+Ly6C^+CD11b^+$) and Macrophages ($CD45^+Lin^-F4/80^+CD11b^-Ly6C^-$) were isolated from spleens. Data are representative of three independent experiments (**b**).

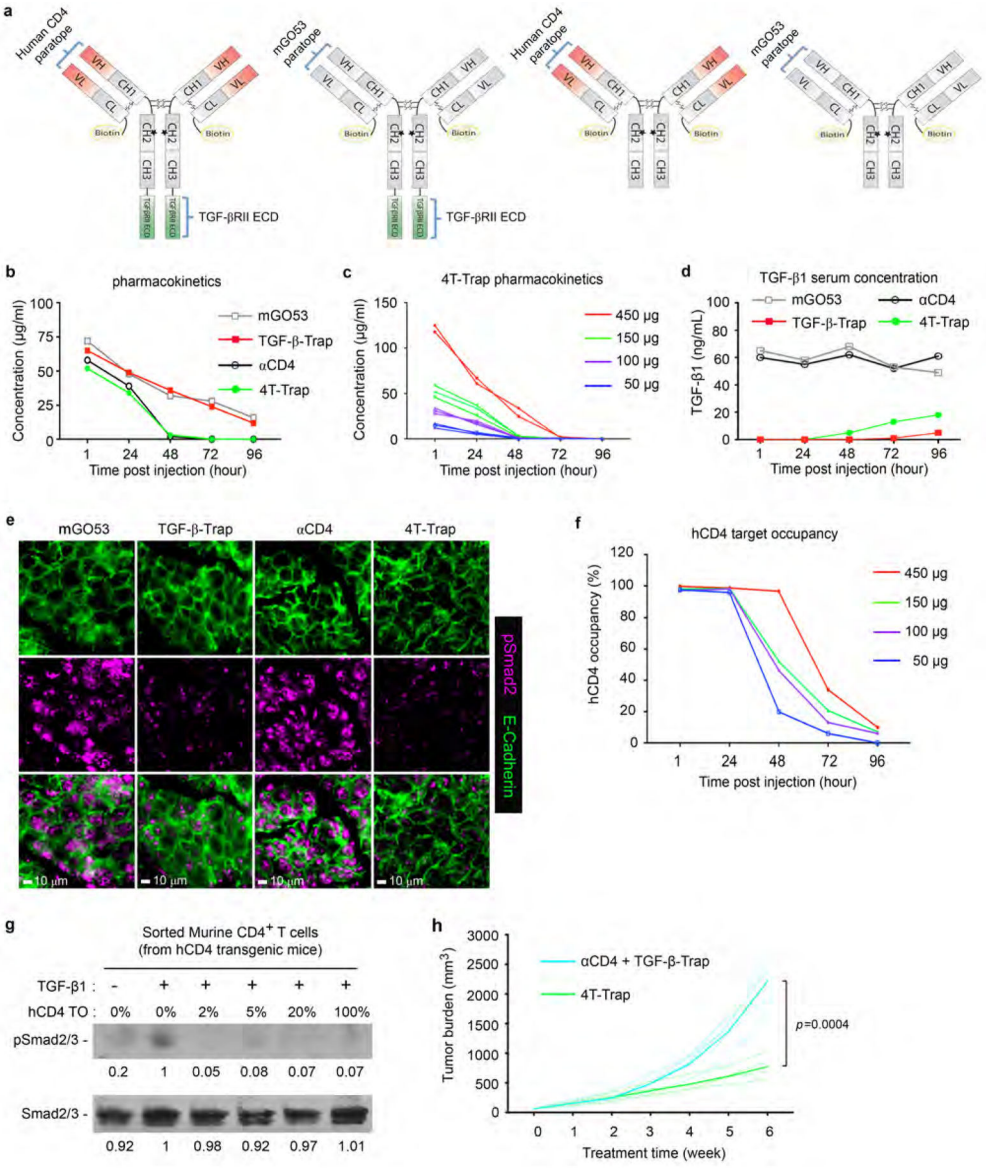

Extended Data Fig. 5 |. Pharmacokinetics, pharmacodynamics and efficacy study of 4T-Trap and control antibodies.

a, Schematic representation of biotinylated 4T-Trap and control antibodies. **b**, Mice were administered with a single dose of 150 μg 4T-Trap, αCD4, TGF-β-Trap or mGO53 by intravenous injection. Antibody serum levels at different time points were measured by ELISA. **c**, Mice were administered with a single dose of 50 μg, 100 μg, 150 μg or 450 μg 4T-Trap by intravenous injection. Antibody serum levels were measured by ELISA. **d**, Mice were administered with a single dose of 150 μg 4T-Trap, αCD4, TGF-β-Trap or mGO53 by intravenous injection. TGF-β1 serum levels were measured by ELISA. **e**, Representative immunofluorescence images of E-Cadherin (green) and phosphorylated Smad2 (pSmad2, magenta) in mammary tumor tissues from mice treated with the indicated antibodies at 12 hr post injection. **f**, Mice were administered with a single dose of 50 μg, 100 μg, 150 μg or 450 μg 4T-Trap by intravenous injection. Percentage of human CD4 molecule occupancy was measured by flow cytometry. **g**, Immunoblotting analyses of TGF-β-induced SMAD2/3 phosphorylation in mouse $CD4^+$ T cells isolated from human CD4 transgenic mice with different levels of 4T-Trap human CD4 (hCD4) target occupancy (TO). Numbers under lanes indicate SMAD2/3 or pSMAD2/3 band intensity. **h**, Tumor measurements from hCD4PyMT mice treated with 4T-Trap (n=4) or combination of αCD4 with TGF-β-Trap (n=5). Two-tailed unpaired *t*-test (**h**). Data are pooled biological replicates (**h**) or representative of three independent experiments (**b-g**).

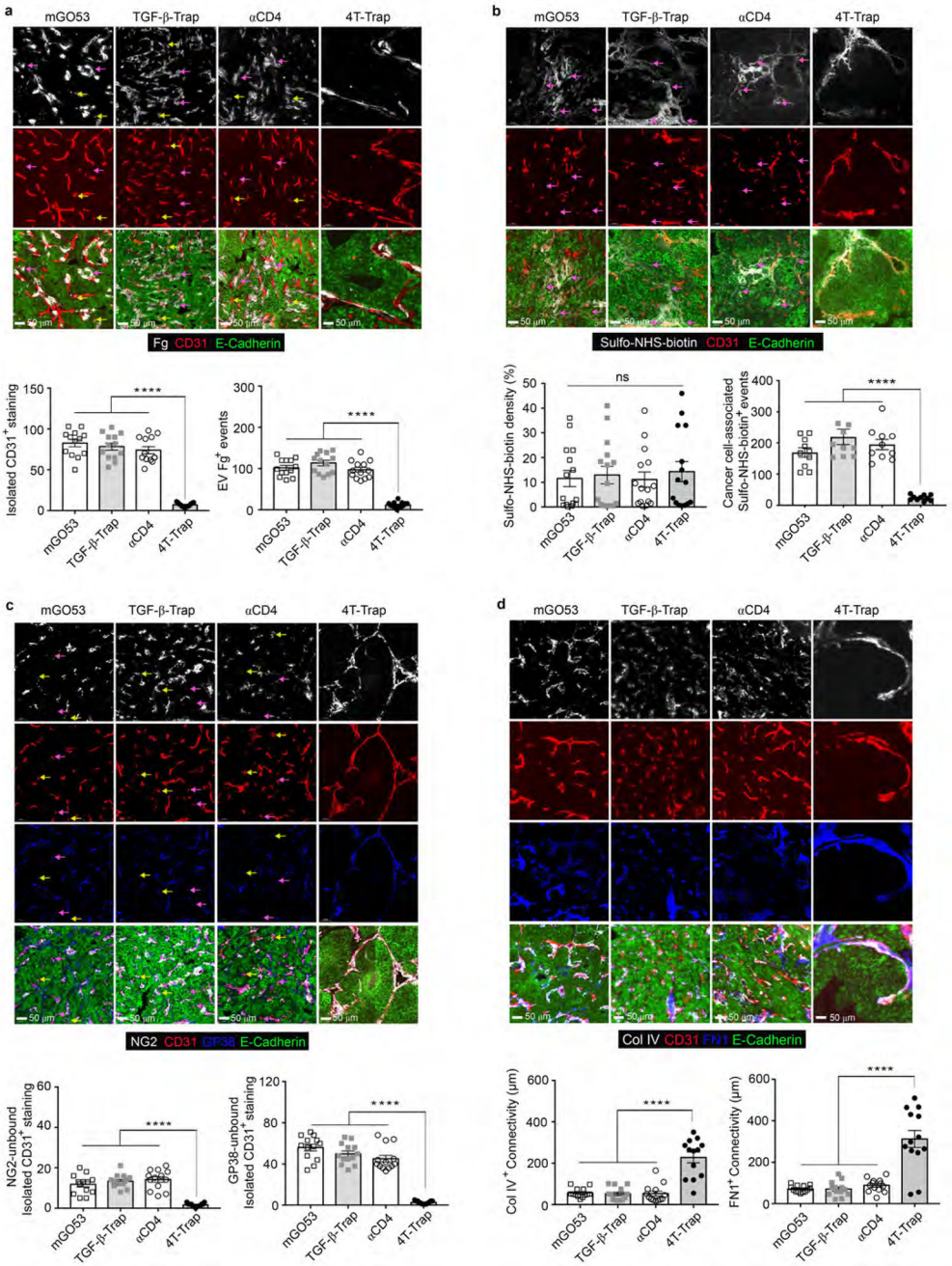

Extended Data Fig. 6 |. 4T-Trap promotes the generation of a reorganized, nonporous and mature tumor vasculature.

a, Representative immunofluorescence images of fibrinogen (Fg, white), CD31 (red) and E-Cadherin (green) in mammary tumor tissues from hCD4PyMT mice treated with 4T-Trap, αCD4, TGF-β-Trap or mGO53 antibodies. Isolated $CD31^+$ staining (yellow arrows) was counted from 1 mm^2 regions (n=13 for each group). Extravascular (EV) Fg deposition events (magenta arrows) were calculated from 1 mm^2 regions (n=13 for each group). **b**, Representative immunofluorescence images of sulfo-NHS-biotin (white), CD31 (red) and E-Cadherin (green) in mammary tumor tissues from hCD4PyMT mice

treated with 4T-Trap, αCD4, TGF-β-Trap or mGO53 antibodies. The percentage of sulfo-NHS-biotin areas over E-Cadherin$^+$ epithelial regions was calculated from 1 mm^2 regions (n=15 for each group). Cancer cell-associated sulfo-NHS-biotin deposition events (magenta arrows) in highly perfused regions were calculated from 1 mm^2 regions (n=10 for each group). **c**, Representative immunofluorescence images of NG2$^+$ pericytes (white), CD31$^+$ endothelial cells (red), GP38$^+$ fibroblasts (cyan) and E-Cadherin (green) in mammary tumor tissues from hCD4PyMT mice treated with 4T-Trap, αCD4, TGF-β-Trap or mGO53 antibodies. NG2-unbound (magenta arrows) or GP38-unbound (yellow arrows) isolated CD31$^+$ staining was counted from 1 mm^2 regions (n=13 for each group). **d**, Representative immunofluorescence images of collagen IV (Col IV, white), CD31 (red), fibronectin (FN, cyan) and E-Cadherin (green) in mammary tumor tissues from hCD4PyMT mice treated with 4T-Trap, αCD4, TGF-β-Trap or mGO53 antibodies. The average continuous lengths of Col IV and FN were measured in 1 mm^2 regions (n=13 for each group). All statistical data are shown as mean ± SEM. ****: P<0.0001 and ns: not significant (one-way ANOVA with *post hoc* Bonferroni *t*-test (**a-d**)). Data are representative of three independent experiments (**a-d**).

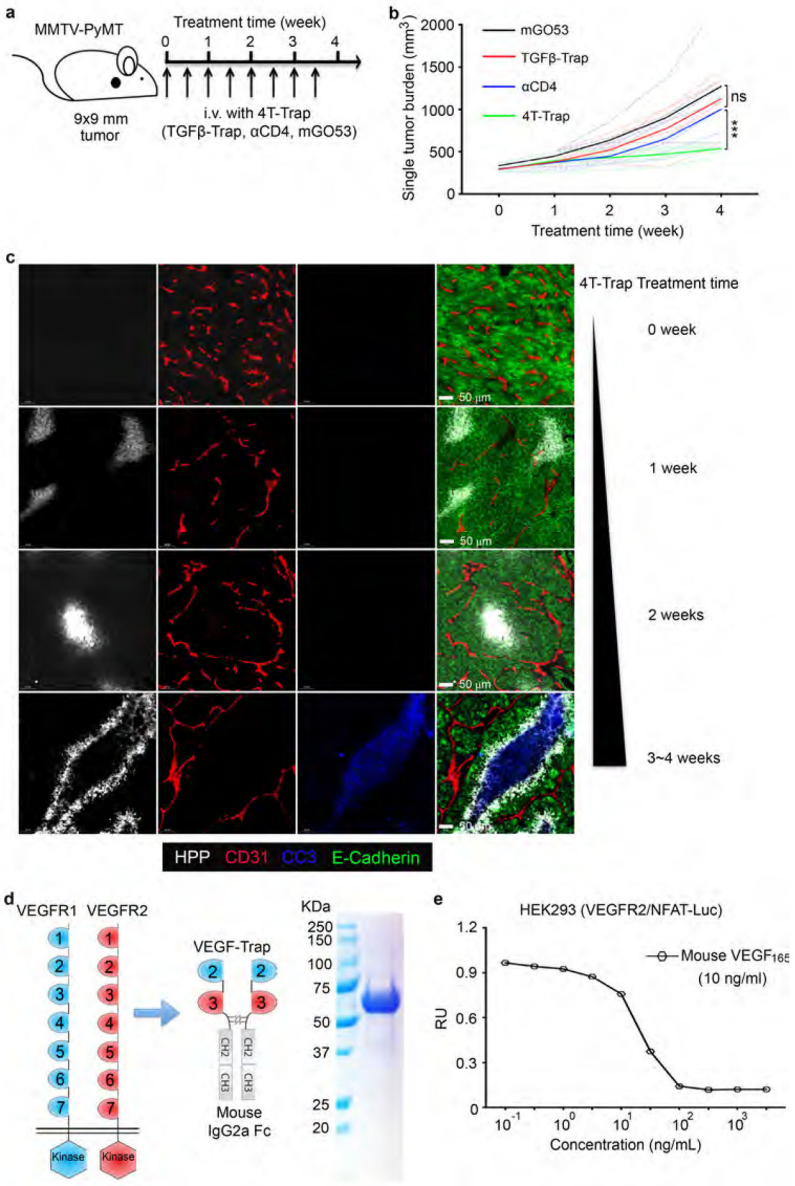

Extended Data Fig. 7 |. 4T-Trap repression of tumor growth and VEGF-Trap construction.

a, A schematic representation of treatment with 4T-Trap and control antibodies. hCD4PyMT mice bearing 9x9 mm tumors were administered with 100 μg antibodies by intravenous injection twice a week for 4 weeks. **b**, Singular tumor measurements from hCD4PyMT mice treated with 4T-Trap, αCD4, TGF-β-Trap or mGO53 (n=7, 6, 7 and 5). **c**, Representative immunofluorescence images of a hypoxia probe (HPP, white), CD31 (red), cleaved Caspase 3 (CC3, blue) and E-Cadherin (green) in mammary tumor tissues from mice treated with 4T-Trap at the indicated time points. **d,** Schematic representation of human VEGFR1, VEGFR2 and VEGF-Trap as well as purity examination of recombinant VEGF-Trap by SDS-PAGE followed by Coomassie Blue staining. **e**, VEGF signaling inhibitory function of VEGF-Trap. HEK293 cells transfected with a VEGF/NFAT firefly luciferase reporter plasmid, together with a VEGFR2 expression plasmid and a pRL-TK Renilla luciferase reporter plasmid, were

incubated with different concentrations of VEGF-Trap for 30 min followed by 10 ng/mL recombinant human $VEGF_{165}$ for 12 hr before subject to the luciferase assay. RU, relative unit of normalized Firefly luciferase activity to Renilla luciferase activity. ***: $P<0.001$ and ns, not significant (one-way ANOVA with *post hoc* Bonferroni *t*-test (**b**)). Data are pooled biological replicates (**b**) or representative of three independent experiments (**c-e**).

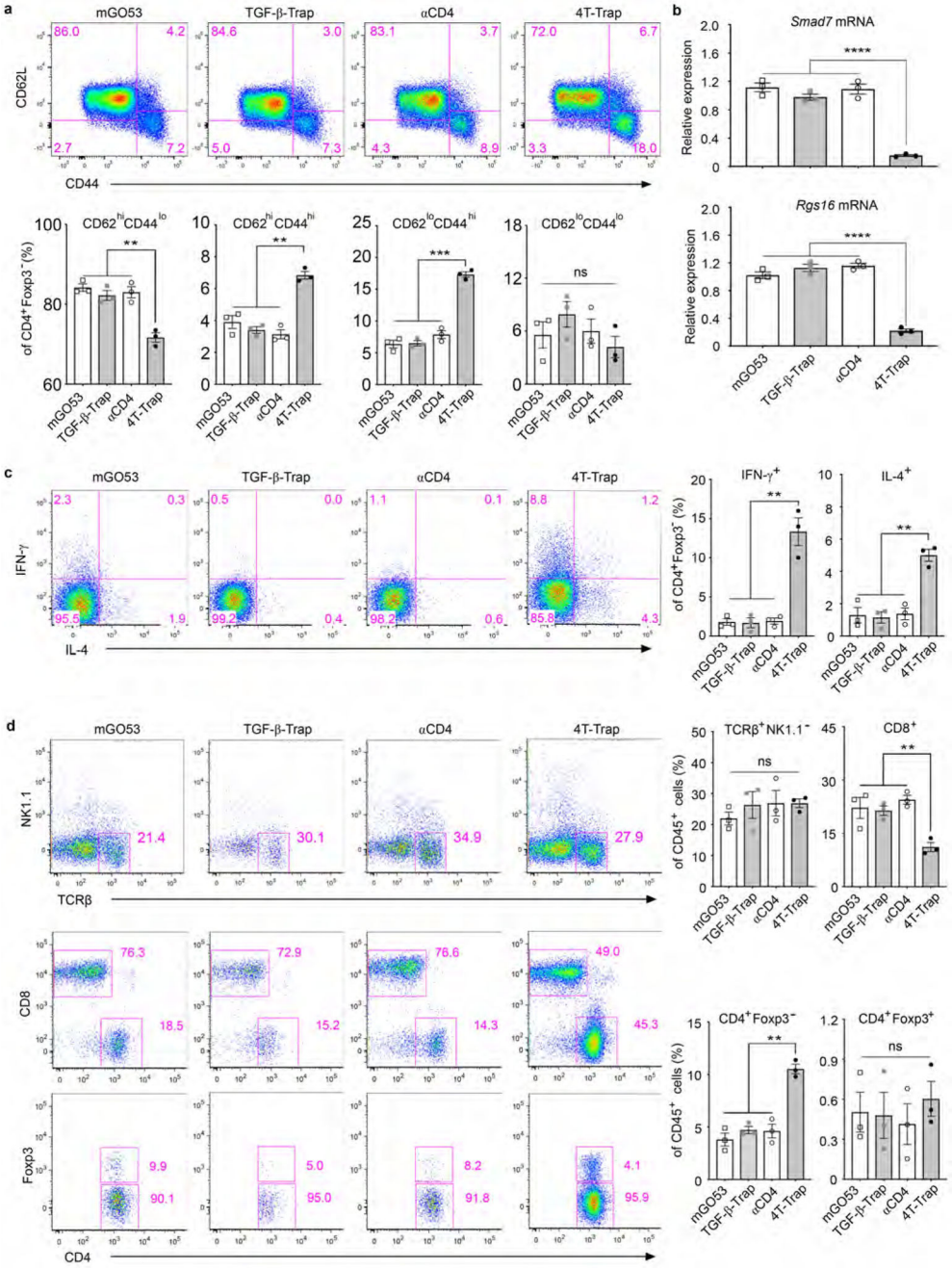

Extended Data Fig. 8 |. 4T-Trap induces T helper cell activation, differentiation and tumor infiltration.

a, Representative flow cytometry plots and statistical analyses of CD62L and CD44 expression in conventional $CD4^+Foxp3^-$ T cells from the tumor-draining lymph nodes of hCD4PyMT mice treated with 4T-Trap, αCD4, TGF-β-Trap or mGO53 antibodies (n=3 for each group). **b**, Quantitative RT-PCR analyses of *Smad7* and *Rgs16* mRNA expression in effector/memory $CD4^+$ T cells from the tumor-draining lymph nodes of hCD4PyMT mice treated with the indicated antibodies. **c**, Representative flow cytometry plots and statistical analyses of IFN-γ and IL-4 expression in conventional $CD4^+Foxp3^-$ T cells from the tumor-draining lymph nodes of hCD4PyMT mice treated with 4T-Trap, αCD4, TGF-β-Trap or mGO53 antibodies (n=3 for each group). **d,** Representative flow cytometry plots and statistical analyses of TCRβ, NK1.1, CD4, CD8 and Foxp3 expression in tumor-infiltrating leukocytes from hCD4PyMT mice treated with 4T-Trap, αCD4, TGF-β-Trap or mGO53 antibodies (n=3 for each group). All statistical data are shown as mean ± SEM. **: $P<0.01$; ***: $P<0.001$; ****: $P<0.0001$ and ns: not significant (one-way ANOVA with *post hoc* Bonferroni *t*-test (**a-d**)). Data are shown as mean ± SEM of three independent biological replicates (**a-d**).

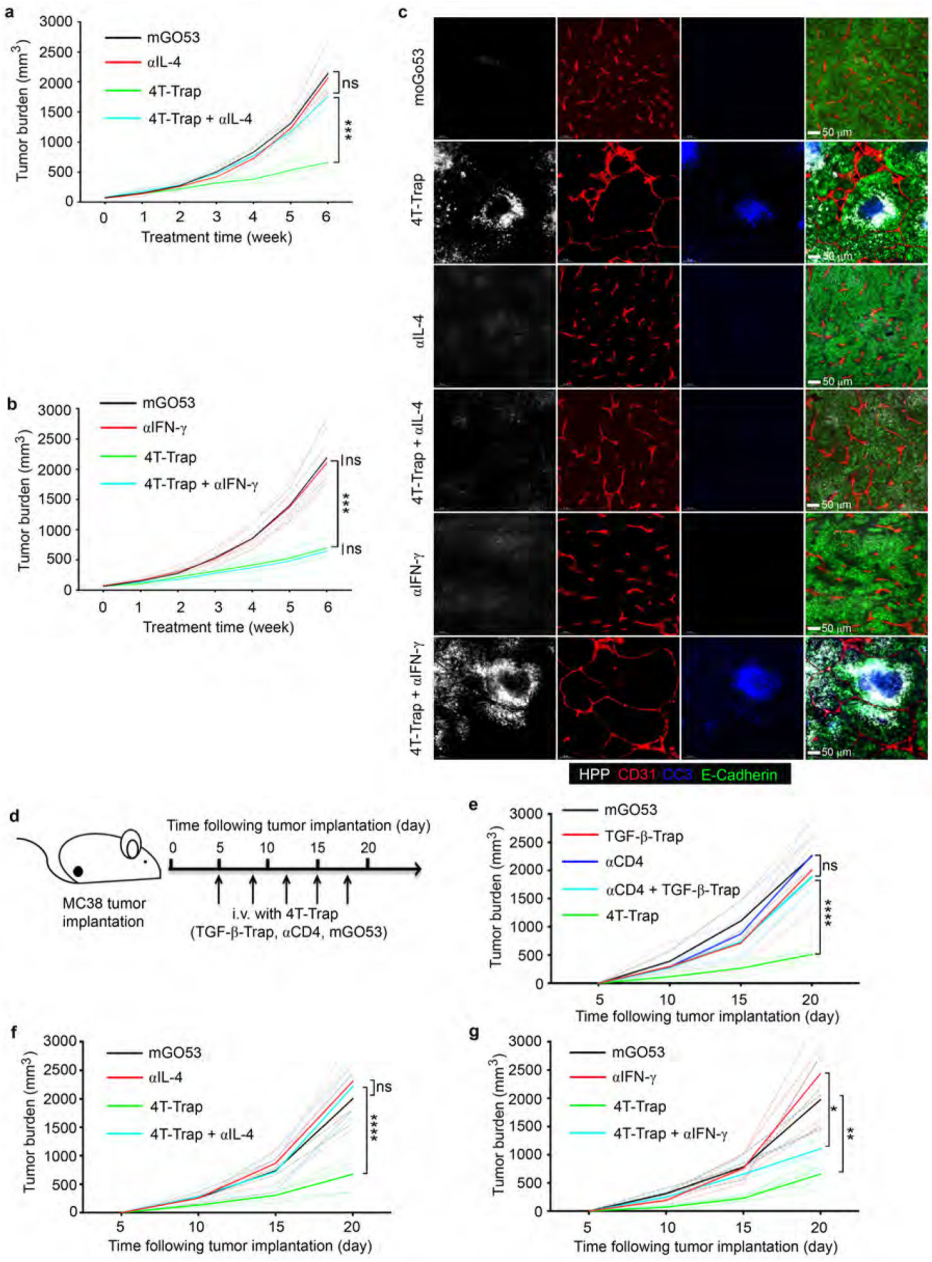

Extended Data Fig. 9 |. 4T-Trap-triggered anti-tumor immunity is dependent on IL-4.

a-b, Tumor measurements from hCD4PyMT mice treated with mGO53 or 4T-Trap in the absence or presence of an IL-4 neutralizing antibody (αIL-4) or an IFN-γ neutralizing antibody (αIFN-γ) (n=5 for each group). **c,** Representative immunofluorescence images of a hypoxia probe (HPP, white), CD31 (red), cleaved Caspase 3 (CC3, blue) and E-Cadherin (green) in mammary tumor tissues from hCD4PyMT mice treated with mGO53 or 4T-Trap in the absence or presence of αIL-4 or αIFN-γ. **d**, Schematic representation of treatment with 4T-Trap and control antibodies. hCD4 mice injected subcutaneously with MC38 cancer cells, were treated with 4T-Trap or control antibodies including TGF-β-Trap, αCD4 and mGO53 (100 μg/dose), for a total of 5 doses. **e**, Tumor measurements from hCD4

mice bearing MC38 cancer cells treated with 4T-Trap, TGF-β-Trap, αCD4, mGO53 and combination of αCD4 with TGF-β-Trap (n=5 for each group). **f**, Tumor measurements from hCD4 mice bearing MC38 cancer cells treated with mGO53, αIL-4, 4T-Trap and combination of αIL-4 with 4T-Trap (n=5 for each group). **g**, Tumor measurements from hCD4 mice bearing MC38 cancer cells treated with mGO53, αIFN-γ, 4T-Trap and combination of αIFN-γ with 4T-Trap (n=5 for each group). *: $P<0.05$; **: $P<0.01$; ***: $P<0.001$, ****: $P<0.0001$ and ns: not significant (two-way ANOVA with *post hoc* Bonferroni *t*-test (**a**, **b**, **e-g**)). Data are pooled biological replicates (**a**, **b**, **e-g**) or representative of three independent experiments (**c**).

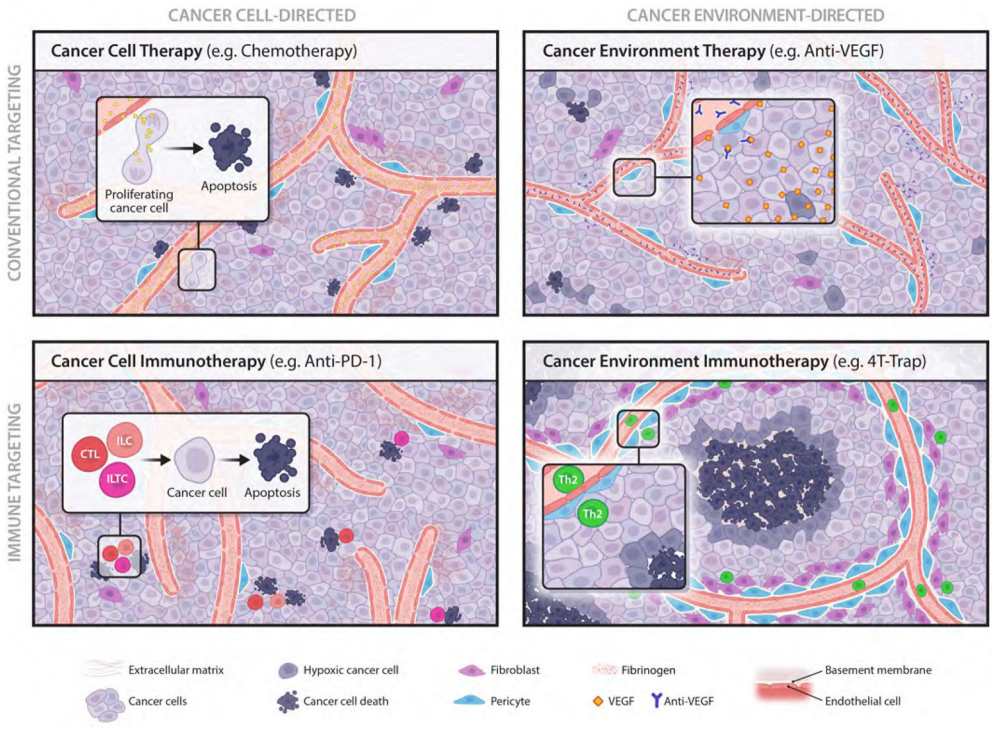

Extended Data Fig. 10 |. Cancer therapy landscape.

Cancer therapies are grouped into four categories in terms of targets and targeting strategies. Cancer cell-directed therapies aim to directly destruct cancer cells, which include conventional *'cancer cell therapy'* with targeting approaches such as chemotherapy to eliminate mitotic cancer cells, and *'cancer cell immunotherapy'* to engage immune effectors such as cytotoxic T lymphocytes (CTLs), killer innate lymphocytes (ILCs) and killer innate-like T cells (ILTCs) to eradicate cancer cells. The cancer immunosurveillance function of CTLs can be revived by immune checkpoint inhibitors such as PD-1 antibodies (anti-PD-1). Cancer environment-directed therapies aspire to rectify the host tissue pathology that fosters tumor growth. A cancer environment hallmark is angiogenesis characterized by a leaky and immature blood vasculature. Conventional *'cancer environment therapy'* includes anti-angiogenics such as VEGF antibodies (anti-VEGF) that diminish vasculature abundance. Blockade of TGF-β signaling in helper T (Th) cells with 4T-Trap results in enhanced Th2 cell differentiation that promotes vasculature remodeling and tumor tissue healing with

cancer cell hypoxia and cancer cell death instigated in avascular regions. 4T-Trap defines a novel modality of *'cancer environment immunotherapy'*.

Supplementary Material

Refer to Web version on PubMed Central for supplementary material.

Acknowledgements

We thank members of the M.O.L. laboratory for helpful discussions, and Shiaoching Gong (MSKCC) for help with the recombineering technique and BAC DNA purification. This work was supported by a Howard Hughes Medical Institute Faculty Scholar Award (M.O.L.), an award from Mr. William H. and Mrs. Alice Goodwin and the Commonwealth Foundation for Cancer Research and the Center for Experimental Therapeutics at Memorial Sloan Kettering Cancer Center (M.O.L.) and a Cancer Center Support Grant (P30 CA08748). S.L., C.C. and X.Z. are Cancer Research Institute Irvington Fellows supported by the Cancer Research Institute. M.H.D. and B.G.N. are recipients of F31 CA210332 and F30 AI29273-03 awards from National Institutes of Health. E.G.S. is a recipient of a Fellowship from the Alan and Sandra Gerry Metastasis and Tumor Ecosystems Center of MSKCC.

Data Availability

Data generated here are included within the paper (and its Supplementary Information files) or are available from the corresponding authors upon reasonable request. Source data for Figs. 1-4 and Extended Data Figs. 1-3 and 5-9 are provided with the paper.

References

1. Sawyers CLShifting paradigms: the seeds of oncogene addiction. Nature medicine15, 1158–1161, doi:10.1038/nm1009-1158 (2009).
2. Allison JPCheckpoints. Cell162, 1202–1205, doi:10.1016/j.cell.2015.08.047 (2015). [PubMed: 26359978]
3. Sabnis AJ & Bivona TG Principles of Resistance to Targeted Cancer Therapy: Lessons from Basic and Translational Cancer Biology. Trends in molecular medicine 25, 185–197, doi:10.1016/j.molmed.2018.12.009 (2019). [PubMed: 30686761]
4. Sharma P, Hu-Lieskovan S, Wargo JA & Ribas A Primary, Adaptive, and Acquired Resistance to Cancer Immunotherapy. Cell 168, 707–723, doi:10.1016/j.cell.2017.01.017 (2017). [PubMed: 28187290]
5. Folkman JTumor angiogenesis: therapeutic implications. The New England journal of medicine285, 1182–1186, doi:10.1056/NEJM197111182852108 (1971). [PubMed: 4938153]
6. Carmeliet P & Jain RK Molecular mechanisms and clinical applications of angiogenesis. Nature 473, 298–307, doi:10.1038/nature10144 (2011). [PubMed: 21593862]
7. Bergers G & Hanahan D Modes of resistance to anti-angiogenic therapy. Nature reviews. Cancer 8, 592–603, doi:10.1038/nrc2442 (2008). [PubMed: 18650835]
8. Apte RS, Chen DS & Ferrara N VEGF in Signaling and Disease: Beyond Discovery and Development. Cell 176, 1248–1264, doi:10.1016/j.cell.2019.01.021 (2019). [PubMed: 30849371]
9. Spitzer MHet al.Systemic Immunity Is Required for Effective Cancer Immunotherapy. Cell168, 487–502 e415, doi:10.1016/j.cell.2016.12.022 (2017). [PubMed: 28111070]
10. Rigamonti Net al.Role of angiopoietin-2 in adaptive tumor resistance to VEGF signaling blockade. Cell reports8, 696–706, doi:10.1016/j.celrep.2014.06.059 (2014). [PubMed: 25088418]
11. Burkly LCet al.Inhibition of HIV infection by a novel CD4 domain 2-specific monoclonal antibody. Dissecting the basis for its inhibitory effect on HIV-induced cell fusion. Journal of immunology149, 1779–1787 (1992).

12. Song Ret al.Epitope mapping of ibalizumab, a humanized anti-CD4 monoclonal antibody with anti-HIV-1 activity in infected patients. Journal of virology84, 6935–6942, doi:10.1128/JVI.00453-10 (2010). [PubMed: 20463063]
13. Bissell MJ & Hines WC Why don't we get more cancer? A proposed role of the microenvironment in restraining cancer progression. Nature medicine 17, 320–329, doi:10.1038/nm.2328 (2011).
14. Huang STumor progression: chance and necessity in Darwinian and Lamarckian somatic (mutationless) evolution. Progress in biophysics and molecular biology110, 69–86, doi:10.1016/j.pbiomolbio.2012.05.001 (2012). [PubMed: 22579660]
15. Dvorak HFTumors: wounds that do not heal. Similarities between tumor stroma generation and wound healing. N Engl J Med315, 1650–1659, doi:10.1056/NEJM198612253152606 (1986). [PubMed: 3537791]
16. Sledzinska Aet al.TGF-beta signalling is required for CD4(+) T cell homeostasis but dispensable for regulatory T cell function. PLoS biology11, e1001674, doi:10.1371/journal.pbio.1001674 (2013). [PubMed: 24115907]
17. Donkor MKet al.T cell surveillance of oncogene-induced prostate cancer is impeded by T cell-derived TGF-beta1 cytokine. Immunity35, 123–134, doi:10.1016/j.immuni.2011.04.019 (2011). [PubMed: 21757379]
18. Sarkar A, Donkor MK & Li MO T cell- but not tumor cell-produced TGF-beta1 promotes the development of spontaneous mammary cancer. Oncotarget 2, 1339–1351, doi:10.18632/oncotarget.403 (2011). [PubMed: 22248703]
19. Donkor MK, Sarkar A & Li MO Tgf-beta1 produced by activated CD4(+) T Cells Antagonizes T Cell Surveillance of Tumor Development. Oncoimmunology 1, 162–171, doi:10.4161/onci.1.2.18481 (2012). [PubMed: 22720237]
20. Killeen N, Sawada S & Littman DR Regulated expression of human CD4 rescues helper T cell development in mice lacking expression of endogenous CD4. The EMBO journal 12, 1547–1553 (1993). [PubMed: 8467804]
21. Semenza GLOxygen sensing, hypoxia-inducible factors, and disease pathophysiology. Annual review of pathology9, 47–71, doi:10.1146/annurev-pathol-012513-104720 (2014).
22. Holash Jet al.VEGF-Trap: a VEGF blocker with potent antitumor effects. Proceedings of the National Academy of Sciences of the United States of America99, 11393–11398, doi:10.1073/pnas.172398299 (2002). [PubMed: 12177445]
23. Flavell RA, Sanjabi S, Wrzesinski SH & Licona-Limon P The polarization of immune cells in the tumour environment by TGFbeta. Nat Rev Immunol 10, 554–567, doi:10.1038/nri2808 (2010). [PubMed: 20616810]
24. Pickup MW, Owens P & Moses HL TGF-beta, Bone Morphogenetic Protein, and Activin Signaling and the Tumor Microenvironment. Cold Spring Harbor perspectives in biology 9, doi:10.1101/cshperspect.a022285 (2017).
25. Colak S & Ten Dijke P Targeting TGF-beta Signaling in Cancer. Trends in cancer 3, 56–71, doi:10.1016/j.trecan.2016.11.008 (2017). [PubMed: 28718426]
26. Batlle E & Massague J Transforming Growth Factor-beta Signaling in Immunity and Cancer. Immunity 50, 924–940, doi:10.1016/j.immuni.2019.03.024 (2019). [PubMed: 30995507]
27. Lan Yet al.Enhanced preclinical antitumor activity of M7824, a bifunctional fusion protein simultaneously targeting PD-L1 and TGF-beta. Science translational medicine10, doi:10.1126/scitranslmed.aan5488 (2018).
28. Ravi Ret al.Bifunctional immune checkpoint-targeted antibody-ligand traps that simultaneously disable TGFbeta enhance the efficacy of cancer immunotherapy. Nature communications9, 741, doi:10.1038/s41467-017-02696-6 (2018).
29. Jiao Set al.Differences in Tumor Microenvironment Dictate T Helper Lineage Polarization and Response to Immune Checkpoint Therapy. Cell179, 1177–1190 e1113, doi:10.1016/j.cell.2019.10.029 (2019). [PubMed: 31730856]

Methods References

31. Ouyang W, Beckett O, Ma Q & Li MO Transforming growth factor-beta signaling curbs thymic negative selection promoting regulatory T cell development. Immunity 32, 642–653, doi:10.1016/j.immuni.2010.04.012 (2010). [PubMed: 20471291]
32. Sarkar A, Donkor MK & Li MO T cell- but not tumor cell-produced TGF-beta1 promotes the development of spontaneous mammary cancer. Oncotarget 2, 1339–1351, doi:10.18632/oncotarget.403 (2011). [PubMed: 22248703]
33. Killeen N, Sawada S & Littman DR Regulated expression of human CD4 rescues helper T cell development in mice lacking expression of endogenous CD4. The EMBO journal 12, 1547–1553 (1993). [PubMed: 8467804]
34. Franklin RAet al.The cellular and molecular origin of tumor-associated macrophages. Science344, 921–925, doi:10.1126/science.1252510 (2014). [PubMed: 24812208]
35. Oh SAet al.Foxp3-independent mechanism by which TGF-beta controls peripheral T cell tolerance. Proceedings of the National Academy of Sciences of the United States of America114, E7536–E7544, doi:10.1073/pnas.1706356114 (2017). [PubMed: 28827353]
36. Holash Jet al.VEGF-Trap: a VEGF blocker with potent antitumor effects. Proceedings of the National Academy of Sciences of the United States of America99, 11393–11398, doi:10.1073/pnas.172398299 (2002). [PubMed: 12177445]
37. Mouquet H, Warncke M, Scheid JF, Seaman MS & Nussenzweig MCEnhanced HIV-1 neutralization by antibody heteroligation. Proceedings of the National Academy of Sciences of the United States of America 109, 875–880, doi:10.1073/pnas.1120059109 (2012). [PubMed: 22219363]
38. Zhou S, Zawel L, Lengauer C, Kinzler KW & Vogelstein B Characterization of human FAST-1, a TGF beta and activin signal transducer. Molecular cell 2, 121–127 (1998). [PubMed: 9702198]
39. Clipstone NA & Crabtree GR Identification of calcineurin as a key signalling enzyme in T-lymphocyte activation. Nature 357, 695–697, doi:10.1038/357695a0 (1992). [PubMed: 1377362]

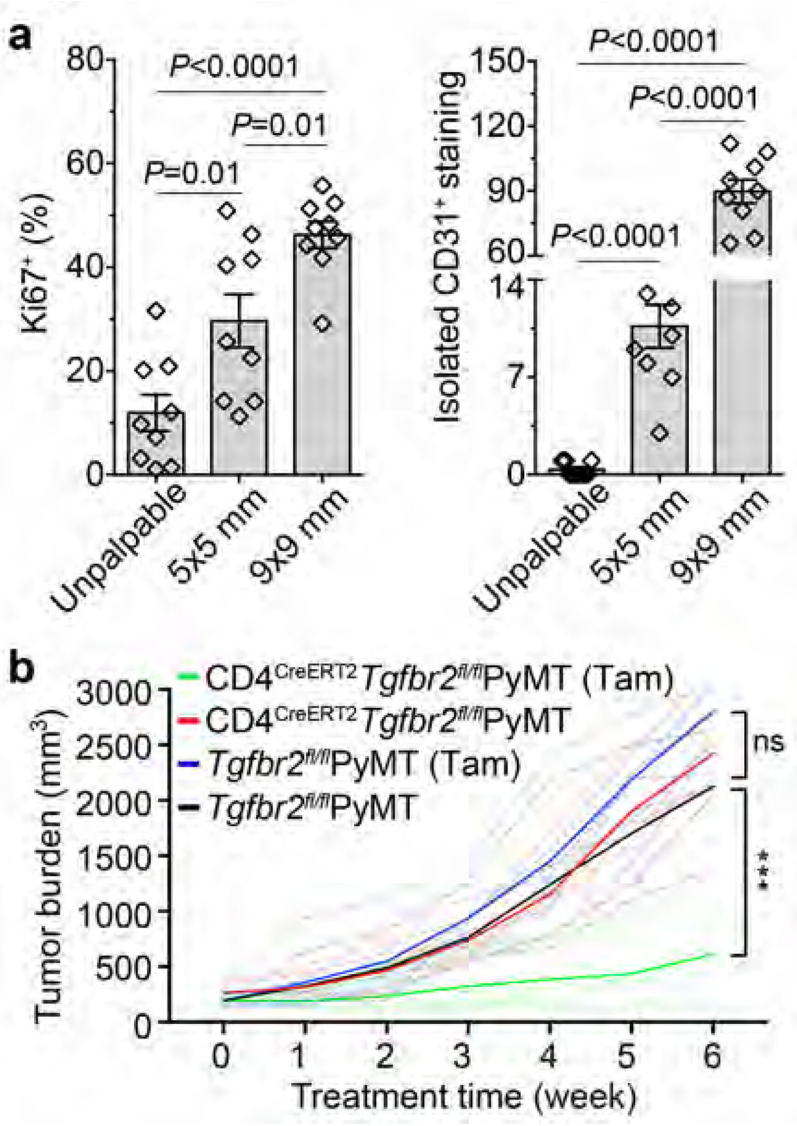

Fig. 1 |. Inducible ablation of TGF-βRII in CD4$^+$ T cells inhibits tumor growth.

a, Statistical analyses of cancer cell proliferation and angiogenesis in tumor tissues from PyMT mice harboring unpalpable, 5x5 mm or 9x9 mm tumors. The percentage of Ki67$^+$E-Cadherin$^+$ cells over total E-Cadherin$^+$ epithelial cells was calculated from 0.02 mm^2 regions (n=9 for each group). Isolated CD31$^+$ staining in the tumor parenchyma was counted from 1 mm^2 regions (n=9 for each group). **b**, *Tgfbr2$^{fl/fl}$*PyMT and CD4^{CreERT2} *Tgfbr2$^{fl/fl}$*PyMT mice bearing 5x5 mm tumors were left untreated or treated with Tamoxifen (Tam) (n=5, 5, 5 and 6) twice a week for 6 weeks. Tumor growth was monitored. Statistical data are shown as mean ± SEM. ***: *P*<0.001 and ns: not significant (one-way (**a**) or two-way ANOVA (**b**) with *post hoc* Bonferroni *t*-test). Data are pooled biological replicates (**b**) or representative of three independent experiments (**a**).

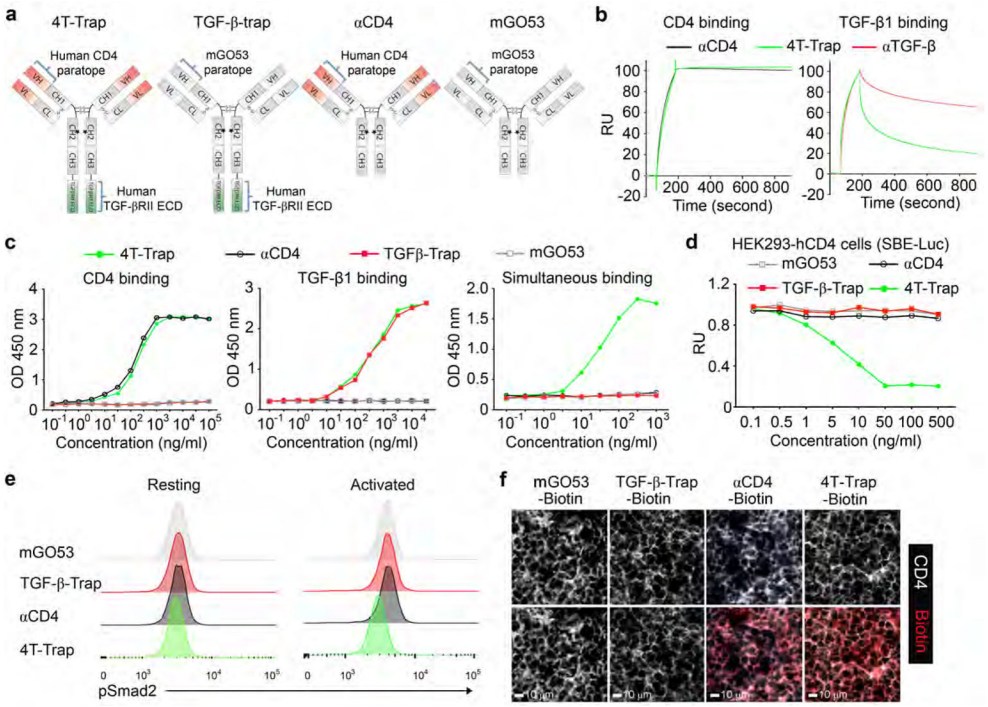

Fig. 2 |. 4T-Trap effectively represses TGF-β signaling in lymph node CD4$^+$ T cells.

a, Schematic representation of antibody structures for 4T-Trap, TGF-β-rap, αCD4 and mGO53. **b**, SPR sensorgrams of 4T-Trap and αCD4 binding to immobilized CD4 (left panel) as well as 4T-Trap and αTGF-β binding to immobilized TGF-β1 (right panel). RU, response unit. **c**, Enzyme-linked immunosorbent assay to assess 4T-Trap, TGF-β-Trap, αCD4 and mGO53 binding to CD4, TGF-β1 or both molecules. Optical densities (OD) were detected at 450 nm. **d**, TGF-β signaling inhibitory functions of the indicated antibodies in HEK293-hCD4 cells transfected with a TGF-β/SMAD Firefly luciferase reporter plasmid and a pRL-TK Renilla luciferase reporter plasmid. RU, relative unit of normalized Firefly luciferase activity to Renilla luciferase activity. **e**, Flow cytometry analyses of pSmad2 expression on resting or activated CD4$^+$ T cells from the tumor-draining lymph nodes of mice treated with the indicated antibodies. CD4$^+$ T cells were left untreated (resting) or treated with PMA/ionomycin for 4 hr (activated) before pSmad2 staining. **f**, Representative immunofluorescence images of CD4 (white) and Biotin (red) staining in the tumor-draining lymph nodes of mice treated with the indicated antibodies. Data are representative of two (**b**) or three independent experiments (**c-f**).

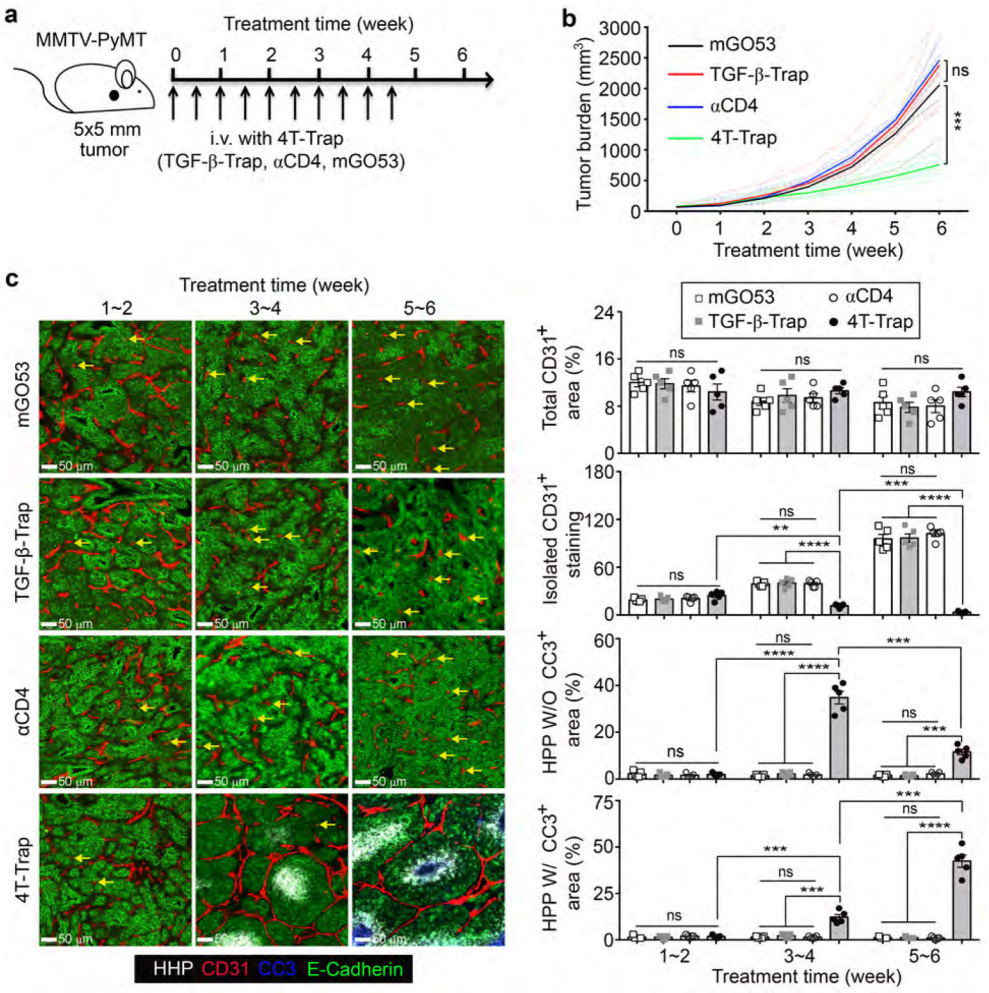

Fig. 3 |. 4T-Trap reprograms the tumor vasculature causing cancer cell hypoxia and cancer cell death.

a, Schematic representation of a treatment scheme with 4T-Trap and control antibodies. hCD4PyMT mice bearing 5x5 mm tumors were administered with 100 μg antibodies by intravenous injection twice a week for 5 weeks. **b**, Tumor measurements from hCD4PyMT mice treated with 4T-Trap, αCD4, TGF-β-Trap or mGO53 (n=8, 5, 10 and 8). **c**, Representative immunofluorescence images of a hypoxia probe (HPP, white), CD31 (red), cleaved Caspase 3 (CC3, blue) and E-Cadherin (green) in tumor tissues from mice treated with the indicated antibodies and time points. The percentage of $CD31^+$ areas, HPP^+ without (W/O) $CC3^+$ areas or HPP^+ with (W/) $CC3^+$ areas over E-Cadherin$^+$ epithelial regions was calculated from 1 mm^2 regions (n=5 for each group). Isolated $CD31^+$ staining (yellow arrows) was counted from 1 mm^2 regions (n=5 for each group). Statistical data are shown as mean ± SEM. **: P<0.01; ***: P<0.001; ****: P<0.0001 and ns: not significant (one-way ANOVA with *post hoc* Bonferroni *t*-test (**b**, **c**)). Data are pooled biological replicates (**b**) or representative of three independent experiments (**c**).

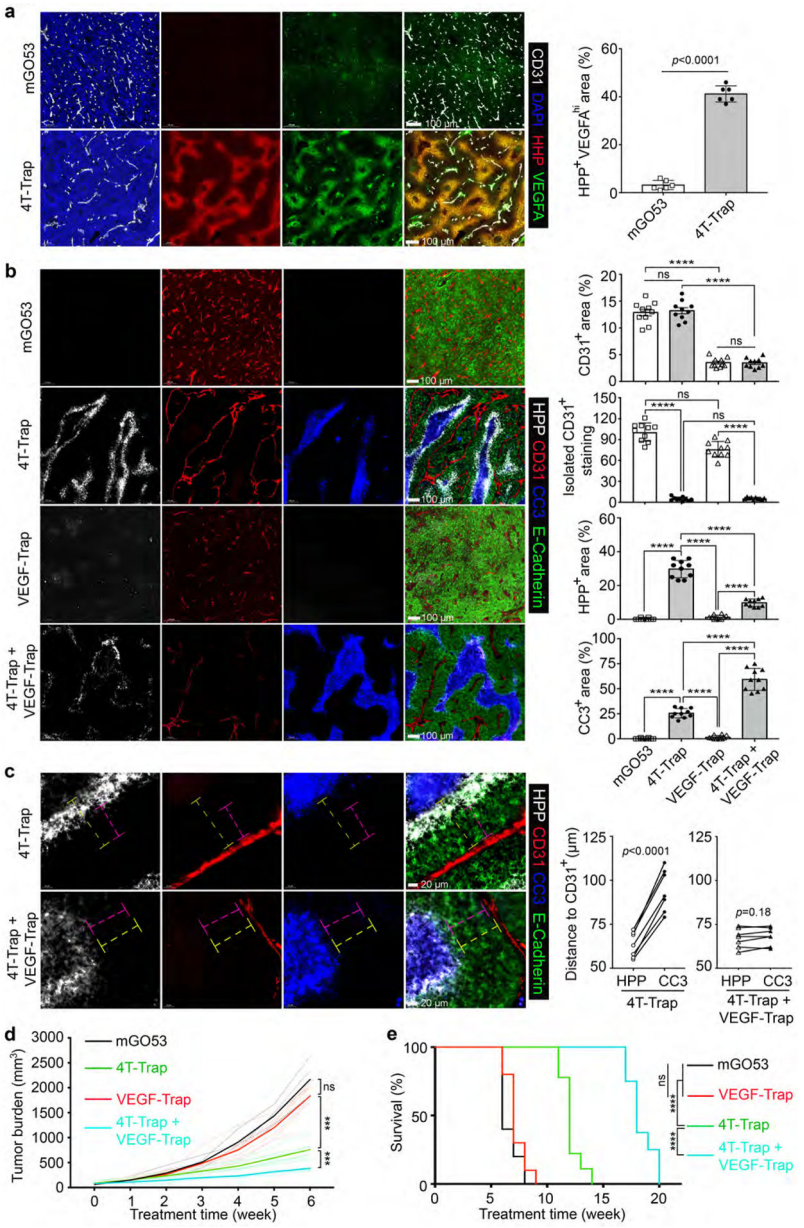

Fig. 4 | 4T-Trap synergizes with VEGF-Trap to induce cancer cell death and suppress tumor growth.

a, Representative immunofluorescence images of CD31 (white), a hypoxia probe (HPP, red) and VEGFA (green) in tumor tissues from hCD4PyMT mice treated with mGO53 or 4T-Trap. The percentage of $HPP^{+}VEGFA^{hi}$ areas was calculated from 1 mm^2 regions (n=6 for each group). **b**, Representative immunofluorescence images of HPP (white), CD31 (red), cleaved Caspase 3 (CC3, blue) and E-Cadherin (green) in tumor tissues from mice treated with the indicated antibodies. The percentage of $CD31^{+}$ areas, HPP^{+} areas or $CC3^{+}$ areas over E-$Cadherin^{+}$ epithelial regions was calculated from 1 mm^2 regions (n=10 for each group). Isolated $CD31^{+}$ staining was counted from 1 mm^2 regions (n=10 for each group). **c**, Representative high magnification immunofluorescence images of HPP (white), CD31 (red), CC3 (blue) and E-Cadherin (green) in tumor tissues from mice treated with

the indicated antibodies. The shortest distance of HPP^+ regions (magenta dashed lines) or $CC3^+$ regions (yellow dashed lines) to $CD31^+$ endothelial cells was measured and plotted (n=7 for each group). **d**, Tumor measurements from hCD4PyMT mice treated with the indicated antibodies (n=7 for each group). **e**, Kaplan-Meier survival curve of hCD4PyMT mice treated with mGO53, 4T-Trap, VEGF-Trap or 4T-Trap and VEGF-Trap (n=10, 9, 10 and 8). Statistical data are shown as mean ± SEM. ***: $P<0.001$; ****: $P<0.0001$ and ns: not significant (two-tailed unpaired *t*-test (**a**) or paired *t*-test (**c**), two-way ANOVA with *post hoc* Bonferroni *t*-test (**b**, **d**) or long-rank test (**e**)). Data are pooled biological replicates (**d**, **e**) or representative of three independent experiments (**a**, **b**, **c**).